SIEMENS

MAGNETOM Flash

The Magazine of MRI

Issue Number 1/2014 | SCMR Edition

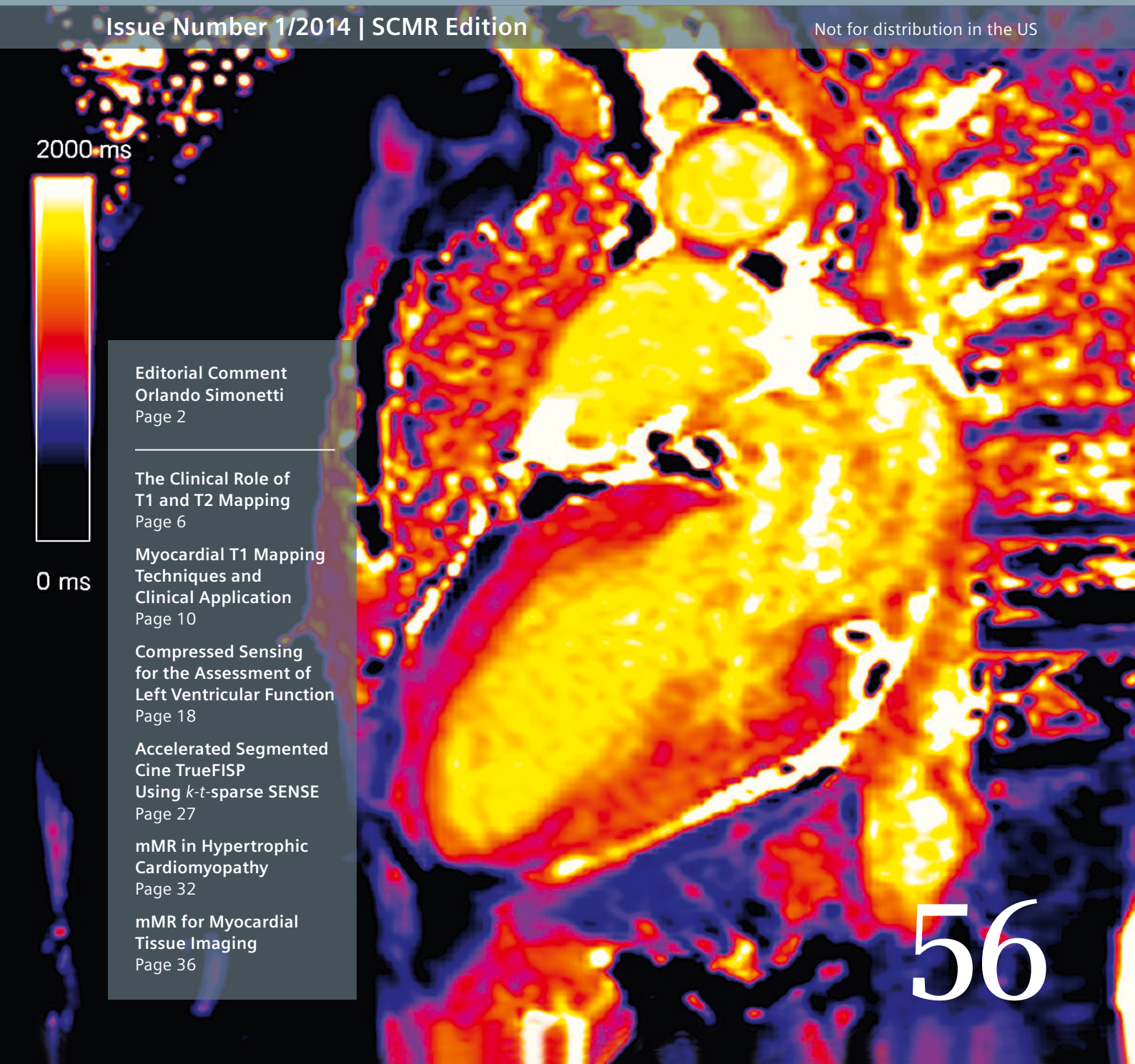

56

Editorial

Orlando P. Simonetti, Ph.D., is a Professor of Internal Medicine and Radiology at The Ohio State University in Columbus, Ohio. He joined the OSU faculty in 2005 as the Research Director of Cardiovascular MR and CT.

His current research interests include fast imaging, flow quantification, parameter mapping, and exercise stress CMR.

Dr. Simonetti has dedicated his entire career to the advancement of cardiovascular magnetic resonance technology, and is widely recognized for his contributions to the field.

"The 3 new technologies of myocardial parameter mapping, CMR-PET, and compressed sensing offer the potential to significantly improve the efficiency and effectiveness of CMR, and to expand the information CMR can provide to physicians to better diagnose and treat cardiovascular disease."

Orlando P. Simonetti, Ph.D.

Dear MAGNETOM Flash reader,

One could easily argue that cardiovascular magnetic resonance (CMR) is in the midst of another technical revolution. Those of us who have worked in the field for the last two decades have seen similar periods in the past, when major advances in hardware technology like array coils and fast gradients, in software technology like parallel acquisition techniques, and pulse sequences like balanced steady-state free precession have spawned dramatic improvements in the efficiency and effectiveness of CMR. Three of the most exciting recent advances: myocardial parameter mapping, MR-PET, and compressed sensing are highlighted in the six articles of this issue of MAGNETOM Flash. Relaxation parameter mapping has initiated an exciting new direction of research into the clinical implications of diffuse changes in myocardial tissue (e.g., fibrosis or edema) that can accompany a variety of diseases. The novel combination of CMR and PET is enabling the powerful diagnostic combination of the exquisite assessment of myocardial tissue structure and function provided by CMR, together with the evaluation of metabolism by PET. New approaches to sampling and reconstruction using compressed sensing are dramatically reducing the data acquisition requirements, and thereby significantly enhancing the efficiency of CMR. Together, these advances are indicative of the ever-changing nature of CMR; a technology that continues to improve thanks to the passion, creativity, and tireless effort of the researchers around the world who have made this their life's work.

The article by Moon et al., from University College London Hospitals, London, UK, discusses recent trends in the development and investigation of techniques for quantitative mapping of myocardial T1 and T2 relaxation parameters. Quantitative mapping addresses many of the technical limitations of conventional T1-weighted and T2-weighted sequences, most importantly offering the capability to assess diffuse changes in myocardial tissue that can accompany many disease states. The article by Fernandes et al., from University of Campinas, Brazil, nicely summarizes the techniques that are employed for myocardial T1 mapping, and reviews recent investigations of this technology in patients with a variety of diseases including amyloid, aortic stenosis, and various cardiomyopathies. As noted in both articles, the early evidence suggests that myocardial relaxation parameter mapping has fantastic potential as a diagnostic tool that may be sensitive to early pathological changes in myocardial tissue potentially missed by other imaging methods. Challenges remain in standardization of these methods to ensure consistent quantitative results across patients and imaging platforms.

The article by Schwitter et al., from the Cardiac Magnetic Resonance Center of the University Hospital of Lausanne in Switzerland nicely demonstrates an important advantage of highly accelerated cine imaging using compressed sensing data acquisition and reconstruction strategies. The ability to acquire sufficient cine slices to cover the entire heart in multiple orientations in a single breath-hold (2 beats per slice) not only reduces exam times, but also facilitates more accurate LV volume calculations using a three dimensional modeling approach rather than the traditional Simpson's Method. Reducing the potential for mis-registration of slices avoids one of the primary limitations of the 3D approach to LV volume calculations. Thus, the efficiency gains achieved via compressed sensing data acquisition and reconstruction strategies can positively impact the clinical value of CMR from several different perspectives.

The article by Carr et al., from the group at Northwestern University in Chicago highlights the tremendous potential of iterative reconstruction techniques to dramatically accelerate cardiac cine imaging. The results shown indicate that efficiency gains of at least a factor of two are possible over conventional parallel acquisition techniques. The time-consuming nature of most CMR techniques, and the requirements of repeated patient breath-holds and regular cardiac rhythm are factors that have constrained the widespread acceptance of CMR into the clinical routine. While there is still work remaining to optimize data sampling and reduce image reconstruction times, the gains in scanning efficiency demonstrated in this study could have far-reaching implications in moving CMR further into the mainstream as a cost-effective diagnostic imaging modality.

The potential advantages of simultaneous CMR and PET acquisitions are explored in two articles of this issue of MAGNETOM Flash. Drs. Cho and Kong from Yeungnam University Hospital, Daegu, South Korea, demonstrate in a patient with hypertrophic cardiomyopathy the ability to characterize myocardial fibrosis using both Late Gadolinium Enhancement and ^{18}F-FDG PET.

The article by Dr. James A. White from The Lawson Health Research Institute, London, Ontario, Canada, nicely describes the potential for advanced myocardial tissue characterization using the synergistic capabilities of CMR and PET. Dr. White points out how the complementary and unique information provided by CMR and PET may better characterize pathological changes in myocardial tissue in diseases such as sarcoidosis. The evaluation of cellular metabolic activity using PET may fill the role that MR spectroscopy has promised but as yet been unable to deliver in the clinical setting. The field of metabolic imaging is rapidly evolving, however, and the continued development of hyperpolarized ^{13}C offers exciting possibilities as well.

In summary, the three new technologies of myocardial parameter mapping, CMR-PET, and compressed sensing discussed in this issue represent some of the most exciting recent advances in CMR. They offer the potential to significantly improve the efficiency and effectiveness of CMR, and to expand the information CMR can provide to physicians to better diagnose and treat cardiovascular disease.

We appreciate your comments.
Please contact us at magnetomworld.med@siemens.com

The entire editorial staff at The Ohio State University and at Siemens Healthcare extends their appreciation to all the radiologists, technologists, physicists, experts and scholars who donate their time and energy – without payment – in order to share their expertise with the readers of MAGNETOM Flash.

MAGNETOM Flash – Imprint

Publisher:
Siemens AG
Medical Solutions
Business Unit Magnetic Resonance,
Karl-Schall-Straße 6, D-91052 Erlangen,
Germany

Guest Editor:
Orlando P. Simonetti, Ph.D.
Professor of Internal Medicine
and Radiology
The Ohio State University,
Columbus, Ohio, USA

Associate Editor: Antje Hellwich
(antje.hellwich@siemens.com)

Editorial Board: Wellesley Were;
Ralph Strecker; Sven Zühlsdorff, Ph.D.;
Gary R. McNeal, MS (BME);
Peter Kreisler, Ph.D.

Production: Norbert Moser, Siemens AG,
Medical Solutions

Layout: independent Medien-Design
Widenmayerstrasse 16, D-80538 Munich,
Germany

Printer: infowerk GmbH
Wiesentalstraße 40, D-90419 Nürnberg,
Germany

MAGNETOM Flash is also available on the internet:

www.siemens.com/magnetom-world

Add a new layer of pixel-based diagnostic information to cardiac diagnoses. Based on HeartFreeze Inline Motion Correction, MyoMaps[1] provides pixel-based myocardial quantification, on the fly. Now address diffuse, myocardial pathologies (T1 Map), cardiac edema (T2 Map) and improve early detection of iron overload (T2* Map) to guide cardiovascular therapy, starting earlier and more efficiently.

T1 Map courtesy of Peter Kellman, National Institutes of Health, Bethesda, USA.

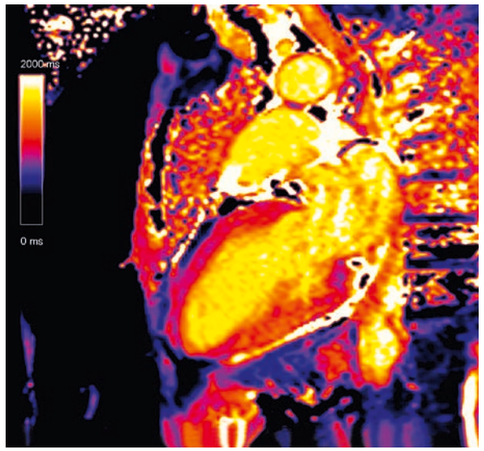

Content

[1]WIP, the product is currently under development and is not for sale in the US and other countries. Its future availability cannot be ensured.

New Generation Cardiac Parametric Mapping: the Clinical Role of T1 and T2 Mapping

Viviana Maestrini; Amna Abdel-Gadir; Anna S. Herrey; James C. Moon

The Heart Hospital Imaging Centre, University College London Hospitals, London, UK

Introduction

Cardiovascular magnetic resonance (CMR) is an essential tool in cardiology and excellent for cardiac function and perfusion. However, a key, unique advantage is its ability to directly scrutinize the fundamental material properties of myocardium – 'myocardial tissue characterization'.

Between 2001 and 2011, the key methods for tissue characterization have been sequences 'weighted' to a magnetic property – T1-weighted imaging for scar (LGE) and T2-weighted for edema (area at risk, myocarditis). These, particularly LGE imaging, have changed our understanding and clinical practice in cardiology.

However, there are limitations to these approaches: Both are difficult to quantify – the LGE technique in particular is very robust in infarction, but harder to quantify in non-ischemic cardiomyopathy. A more fundamental difference is that sequences are designed to optimize contrast between 'normal' and abnormal – a dichotomy of health and disease. As a result, global myocardial pathologies such as diffuse infiltration (fibrosis, amyloid, iron, fat, pan-inflammation) are missed.

Recently, rapid technical innovations have generated new 'mapping' techniques. Rather than being 'weighted', these create a pixel map where each pixel value is the T1 or T2 (or T2*), displayed in color. These new sequences are single breath-hold, increasingly robust and now widely available. With T1 mapping, clever contrast agent use also permits the measurement of the extracellular volume (ECV), quantifying the interstitium (odema, fibrosis or amyloid), also as a map. Early results with these methodologies are exciting – potentially representing a new era of CMR.

T1 mapping

Initial T1 measurement methods were multi-breath-hold. These were time consuming and clunky, but were able to measure well diffuse myocardial fibrosis, a fundamental myocardial property with high potential clinical significance [1]. Healthy volunteers and those with disease had different extents of diffuse fibrosis [2], and these were shown to be clinically significant in a number of diseases. T1 mapping methods based on the MOLLI* approach with modifications for shorter breath-holds, better heart rate independence and better image registration for cleaner maps, however, transformed the field – albeit still with a variety of potential sequences in use [3-5]. There are two key ways of using T1 mapping: Without (or before) contrast – Native T1 mapping; and with contrast, typically by subtracting the pre and post maps with hematocrit correction to generate the ECV [6].

* The product is currently under development; is not for sale in the U.S. and other countries, and its future availability cannot be ensured.

Native T1

Native T1 mapping (pre-contrast T1) can demonstrate intrinsic myocardial contrast (Fig. 1). T1, measured in milliseconds, is higher where the extracellular compartment is increased. Fibrosis (focal, as in infarction, or diffuse) [7-8], odema [9-10] and amyloid [11], are examples. T1 is lower in lipid (Anderson Fabry disease, AFD) [12], and iron [13] accumulation.

These changes are large in some rare disease. Global myocardial changes are robustly detectable without contrast, even in early disease. In iron, AFD and amyloid, changes appear before any other abnormality – there may be no left ventricular hypertrophy, a normal electrocardiogram, and normal conventional CMR, for example – genuinely new information. In established disease, low T1 values in AFD appear to absolutely distinguish it from other causes of left ventricular hypertrophy [12] whilst in established amyloid T1 elevation tracks known markers of cardiac severity [11].

A note of caution, however. Native T1, although stable between healthy volunteers to 1 part in 30, is dependent on platform (magnet manufacturer, sequence and sequence variant, field strength) [14]. Normal reference ranges for your setup are needed.

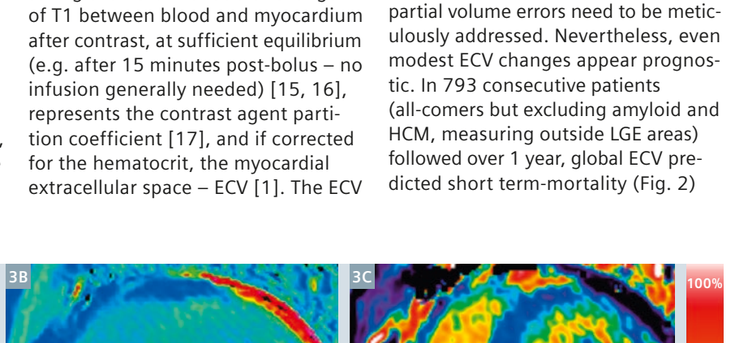

2 ECV in non scar areas (LGE excluded) is associated with all-cause mortality [21].

The signal acquired is also a composite signal – generated by both interstitium and myocytes. The use of an extracellular contrast agent adds another dimension to T1 mapping and the ability to characterize the extracellular compartment specifically.

Extracellular volume (ECV)

Initially, post-contrast T1 was measured, but this is confounded by renal clearance, gadolinium dose, body composition, acquisition time post bolus, and hematocrit. Better is measuring the ECV. The ratio of change of T1 between blood and myocardium after contrast, at sufficient equilibrium (e.g. after 15 minutes post-bolus – no infusion generally needed) [15, 16], represents the contrast agent partition coefficient [17], and if corrected for the hematocrit, the myocardial extracellular space – ECV [1]. The ECV is specific for extracellular expansion, and well validated. Clinically this occurs in fibrosis, amyloid and odema. To distinguish, the degree of ECV change and the clinical context is important. A multiparametric approach (e. g. T2 mapping or T2-weighted imaging in addition) may therefore be useful. Amyloid can have far higher ECVs than any other disease [18] whereas ageing has small changes – near the detection limits, but of high potential clinical importance [19, 20]. For low ECV expansion diseases, biases from blood pool partial volume errors need to be meticulously addressed. Nevertheless, even modest ECV changes appear prognostic. In 793 consecutive patients (all-comers but excluding amyloid and HCM, measuring outside LGE areas) followed over 1 year, global ECV predicted short term-mortality (Fig. 2)

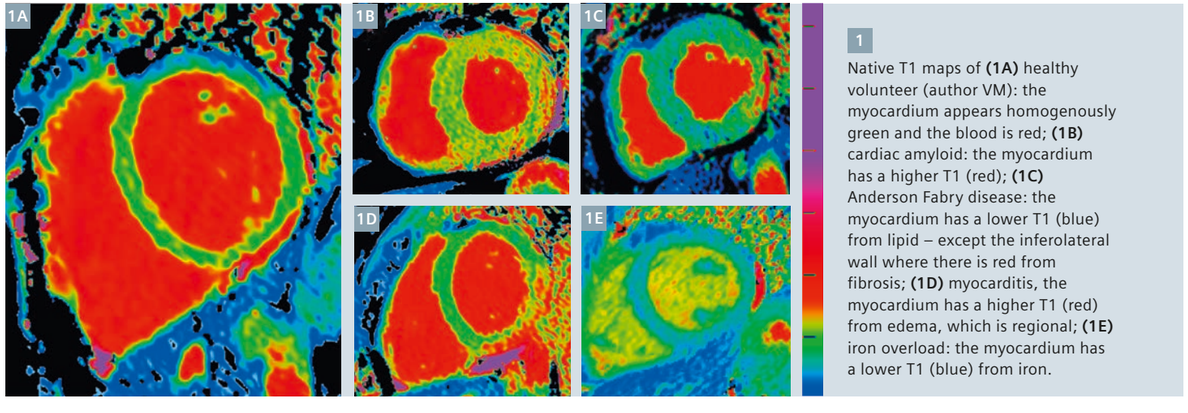

1 Native T1 maps of **(1A)** healthy volunteer (author VM): the myocardium appears homogenously green and the blood is red; **(1B)** cardiac amyloid: the myocardium has a higher T1 (red); **(1C)** Anderson Fabry disease: the myocardium has a lower T1 (blue) from lipid – except the inferolateral wall where there is red from fibrosis; **(1D)** myocarditis, the myocardium has a higher T1 (red) from edema, which is regional; **(1E)** iron overload: the myocardium has a lower T1 (blue) from iron.

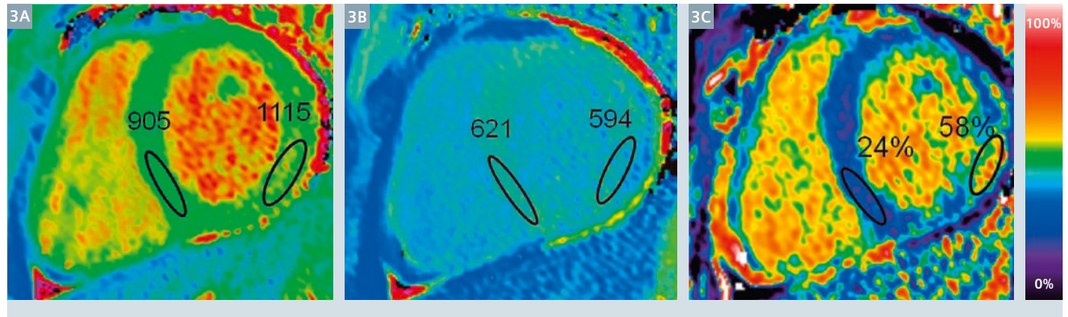

3 A patient with myocarditis. On the left side a native T1 map showing the higher T1 value in the inferolateral wall (1115 ms); in the centre, a post-contrast T1 map showing the shortened T1 value after contrast administration (594 ms); on the right side the derived ECV map showing higher value of ECV (58%) compared to remote myocardium.

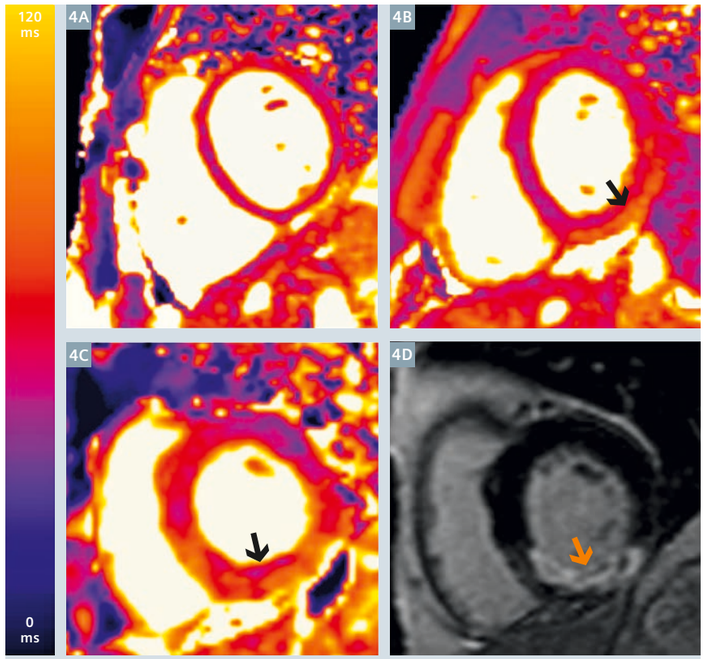

4 **(4A)** T2 mapping in a normal volunteer (author VM). **(4B)** High T2 value in patient with myocarditis – here epicardial edema. **(4C)** Edema in acute myocardial infarction – here patchy due to microvascular obstruction – see LGE, **(4D)**.

[21]. The same group also found (n ~1000) higher ECVs in diabetics. Those on renin-angiotensin-aldosterone system blockade had lower ECVs. ECV also predicted mortality and/or incident hospitalization for heart failure in diabetics [22].

The use and capability of ECV quantification is growing. T1 mapping is getting better and inline ECV maps are now possible where each pixel carries directly the ECV value (Fig. 3) – a more biologically relevant figure than T1 [6].

T2 mapping

T2-weighted CMR identifies myocardial odema both in inflammatory pathologies and acute ischemia, delineating the area at risk. However, these imaging techniques (e. g. STIR) are fragile in the heart and can be challenging, both to acquire and to interpret. Preliminary advances were made with T2-weighted SSFP sequences, which reduce false negatives and positives [23, 24]. T2 mapping seems a further increment [25] (Fig. 4). As with T1 mapping, global diseases such as pan-myocarditis may now be identified by T2 mapping, and preliminary results are showing this in several rheumatologic diseases (lupus, systemic capillary leak syndrome) and transplant rejection, detecting early rejection missed by other modalities [26, 27].

Conclusion

Mapping – T1, T2, ECV mapping of myocardium is an emerging topic with the potential to be a powerful tool in the identification and quantification of diffuse myocardial processes without biopsy. Early evidence suggests that this technique detects early stage disease missed by other imaging methods and has potential as a prognosticator, as a surrogate endpoint in trials, and to monitor therapy. Progress is rapid; challenges remain. Delivery across sites and standardization is now beginning with new draft guidelines for T1 mapping in preparation. Watch this space.

References

1 Flett AS, Hayward MP, Ashworth MT, Hansen MS, Taylor AM, Elliott PM, McGregor C, Moon JC. Equilibrium Contrast Cardiovascular Magnetic Resonance for the measurement of diffuse myocardial fibrosis: preliminary validation in humans. Circulation 2010;122:138-144.

2 Sado DM, Flett AS, Banypersad SM, White SK, Maestrini V, Quarta G, Lachmann RH, Murphy E, Mehta A, Hughes DA, McKenna WJ, Taylor AM, Hausenloy DJ, Hawkins PN, Elliott PM, Moon JC. Cardiovascular magnetic resonance measurement of myocardial extracellular volume in health and disease. Heart 2012;98:1436-1441.

3 Piechnik SK, Ferreira VM, Dall'Armellina E, Cochlin LE, Greiser A, Neubauer S, Robson MD. Shortened Modified Look-Locker Inversion recovery (ShMOLLI) for clinical myocardial T1 mapping at 1.5 and 3 T within a 9 heartbeat breathhold. J Cardiovasc Magn Reson 2010;12:69.

4 Messroghli DR, Greiser A, Fröhlich M, Dietz R, Schulz-Menger J. Optimization and validation of a fully-integrated pulse sequence for modified look-locker inversion-recovery (MOLLI) T1 mapping of the heart. J Magn Reson Imaging 2007;26:1081–1086.

5 Fontana M, White SK, Banypersad SM, Sado DM, Maestrini V, Flett AS, Piechnik SK, Neubauer S, Roberts N, Moon JC. Comparison of T1 mapping techniques for ECV quantification. Histological validation and reproducibility of ShMOLLI versus multibreath-hold T1 quantification equilibrium contrast CMR. J Cardiovasc Magn Reson 201;14:88.

6 Kellman P, Wilson JR, Xue H, Ugander M, Arai AE. Extracellular volume fraction mapping in the myocardium, part 1: evaluation of an automated method. J Cardiovasc Magn Reson 2012;14:63.

7 Dass S, Suttie JJ, Piechnik SK, Ferreira VM, Holloway CJ, Banerjee R, Mahmod M, Cochlin L, Karamitsos TD, Robson MD, Watkins H, Neubauer S. Myocardial tissue characterization using magnetic resonance non contrast T1 mapping in hypertrophic and dilated cardiomyopathy. Circ Cardiovasc Imaging. 2012; 6:726-33.

8 Puntmann VO, Voigt T, Chen Z, Mayr M, Karim R, Rhode K, Pastor A, Carr-White G, Razavi R, Schaeffter T, Nagel E. Native T1 mapping in differentiation of normal myocardium from diffuse disease in hypertrophic and dilated cardiomyopathy. J Am Coll Cardiovasc Imgaging 2013;6:475–84.

9 Ferreira VM, Piechnik SK, Dall'Armellina E, Karamitsos TD, Francis JM, Choudhury RP, Friedrich MG, Robson MD, Neubauer S. Non-contrast T1 mapping detects acute myocardial edema with high diagnostic accuracy: a comparison to T2-weighted cardiovascular magnetic resonance. J Cardiovasc Magn Reson 2012; 14:42.

10 Dall'Armellina E, Piechnik SK, Ferreira VM, Si Ql, Robson MD, Francis JM, Cuculi F, Kharbanda RK, Banning AP, Choudhury RP, Karamitsos TD, Neubauer S. Cardiovascular magnetic resonance by non contrast T1 mapping allows assessment of severity of injury in acute myocardial infarction. J Cardiovasc Magn Reson 2012;14:15.

11 Karamitsos TD, Piechnik SK, Banypersad SM, Fontana M, MD, Ntusi NB, Ferreira VM, Whelan CJ, Myerson SG, Robson MD, Hawkins PN, Neubauer S, Moon JC. Non-contrast T1 Mapping for the Diagnosis of Cardiac Amyloidosis. J Am Coll Cardiol Img 2013;6:488–97.

12 Sado DM, White SK, Piechnik SK, Banypersad SM, Treibel T, Captur G, Fontana M, Maestrini V, Flett AS, Robson MD, Lachmann RH, Murphy E, Mehta A, Hughes D, Neubauer S, Elliott PM, Moon JC. Identification and assessment of Anderson-Fabry Disease by Cardiovascular Magnetic Resonance Non-contrast myocardial T1 Mapping clinical perspective. Circ Cardiovasc Imaging 2013;6:392-398.

13 Pedersen SF, Thrys SA, Robich MP, Paaske WP, Ringgaard S, Bøtker HE, Hansen ESS, Kim WY. Assessment of intramyocardial hemorrhage by T1-weighted cardiovascular magnetic resonance in reperfused acute myocardial infarction. J Cardiovasc Magn Reson 2012; 14:59.

14 Raman FS, Kawel-Boehm N, Gai N, Freed M, Han J, Liu CY, Lima JAC, Bluemke DA, Liu S. Modified look-locker inversion recovery T1 mapping indices: assessment of accuracy and reproducibility between magnetic resonance scanners. J Cardiovasc Magn Reson 2013; 15:64.

15 White SK, Sado DM, Fontana M, Banypersad SM, Maestrini V, Flett AS, Piechnik SK, Robson MD, Hausenloy DJ, Sheikh AM, Hawkins PN, Moon JC. T1 Mapping for Myocardial Extracellular Volume measurement by CMR: Bolus Only Versus Primed Infusion Technique, 2013 Apr 5 [Epub ahead of print].

16 Schelbert EB, Testa SM, Meier CG, Ceyrolles WJ, Levenson JE, Blair AJ, Kellman P, Jones BL, Ludwig DR, Schwartzman D, Shroff SG, Wong TC. Myocardial extravascular extracellular volume fraction measurement by gadolinium cardiovascular magnetic resonance in humans: slow infusion versus bolus. J Cardiovasc Magn Reson 2011, Mar 4;13-16.

17 Flacke SJ, Fischer SE, Lorenz CH. Measurement of the gadopentetate dimeglumine partition coefficient in human myocardium in vivo: normal distribution and elevation in acute and chronic infarction. Radiology 2001;218:703-10.

18 Banypersad SM, Sado DM, Flett AS, Gibbs SDG, Pinney JH, Maestrini V, Cox AT, Fontana M, Whelan CJ, Wechalekar AD, Hawkins PN, Moon JC. Quantification of myocardial extracellular volume fraction in systemic AL amyloidosis: An Equilibrium Contrast Cardiovascular Magnetic Resonance Study. Circ Cardiovasc Imaging 2013;6:34-39.

19 Ugander M, Oki AJ, Hsu LY, Kellman P, Greiser A, Aletras AH, Sibley CT, Chen MY, Bandettini WP, Arai AE. Extracellular volume imaging by magnetic resonance imaging provides insights into overt and sub-clinical myocardial pathology. Eur Heart J 2012; 33: 1268–1278.

20 Liu CY, Chang Liu Y, Wu C, Armstrong A, Volpe GJ, van der Geest RJ, Liu Y, Hundley WG, Gomes AS, Liu S, Nacif M, Bluemke DA, Lima JAC. Evaluation of age related interstitial myocardial fibrosis with Cardiac Magnetic Resonance Contrast-Enhanced T1 Mapping in the Multi-ethnic Study of Atherosclerosis (MESA). J Am Coll Cardiol 2013 Jul 3 [Epub ahead of print].

21 Wong TC, Piehler K, Meier CG, Testa SM, Klock AM, Aneizi AA, Shakesprere J, Kellman P, Shroff SG, Schwartzman DS, Mulukutla SR, Simon MA, Schelbert EB. Association between extracellular matrix expansion quantified by cardiovascular magnetic resonance and short-term mortality. Circulation 2012 Sep 4;126(10):1206-16.

22 Wong TC, Piehler KM, Kang IA, Kadakkal A, Kellman P, Schwartzman DS, Mulukutla SR, Simon MA, Shroff SG, Kuller LH, Schelbert EB. Myocardial extracellular volume fraction quantified by cardiovascular magnetic resonance is increased in diabetes and associated with mortality and incident heart failure admission. Eur Heart J 2013 Jun 11 [Epub ahead of print].

23 Giri S, Chung YC, Merchant A, Mihai G, Rajagopalan S, Raman SV, Simonetti OP. T2 quantification for improved detection of myocardial edema. J Cardiovasc Magn Reson 2009; 11:56.

24 Verhaert D, Thavendiranathan P, Giri S, Mihai G, Rajagopalan S, Simonetti OP, Raman SV. Direct T2 Quantification of Myocardial Edema in Acute Ischemic Injury. J Am Coll Cardiol Img 2011;4: 269-78.

25 Ugander M, Bagi PS, Oki AB, Chen B, Hsu LY, Aletras AH, Shah S, Greiser A, Kellman P, Arai AE. Myocardial oedema as detected by Pre-contrast T1 and T2 CMR delineates area at risk associated with acute myocardial infarction. J Am Coll Cardiol Img 2012;5:596–603.

26 ThavendiranathanP, Walls M, Giri S, Verhaert D, Rajagopalan S, Moore S, Simonetti OP, Raman SV. Improved detection of myocardial involvement in acute inflammatory cardiomyopathies using T2 Mapping. Circ Cardiovasc Imaging 2012;5:102-110.

27 Usman AA, Taimen K, Wasielewski M, McDonald J, Shah S, Shivraman G, Cotts W, McGee E, Gordon R, Collins JD, Markl M, Carr JC. Cardiac Magnetic Resonance T2 Mapping in the monitoring and follow-up of acute cardiac transplant rejection: A Pilot Study. Circ Cardiovasc Imaging. 2012; 6:782-90.

Contact

Dr. James C. Moon
The Heart Hospital Imaging Centre
University College London Hospitals
16–18 Westmoreland Street
London W1G 8PH
UK
Phone: +44 (20) 34563081
Fax: +44 (20) 34563086
james.moon@uclh.nhs.uk

Reprinted from MAGNETOM Flash 5/2013

Reprinted from MAGNETOM Flash 5/2013

Myocardial T1 Mapping: Techniques and Clinical Applications

Juliano Lara Fernandes[1]; Ralph Strecker[2]; Andreas Greiser[3]; Jose Michel Kalaf[1]

[1]Radiologia Clinica de Campinas; University of Campinas, Brazil
[2]Healthcare MR, Siemens Ltda, Sao Paulo, Brazil
[3]MR Cardiology, Siemens Healthcare, Erlangen, Germany

Introduction

Cardiovascular magnetic resonance (CMR) has been an increasingly used imaging modality which has experienced significant advancements in the last years [1]. One of the most used techniques that have made CMR so important is late gadolinium enhancement (LGE) and the demonstration of localized areas of infarct and scar tissue [2–4]. However, despite being very sensitive to small areas of regional fibrosis, LGE techniques are mostly dependent on the comparison to supposedly normal reference areas of myocardium, thus not being able to depict more diffuse disease.

Myocardial interstitial fibrosis, with a diffuse increase in collagen content in myocardial volume, develops as a result of many different stimuli includ-

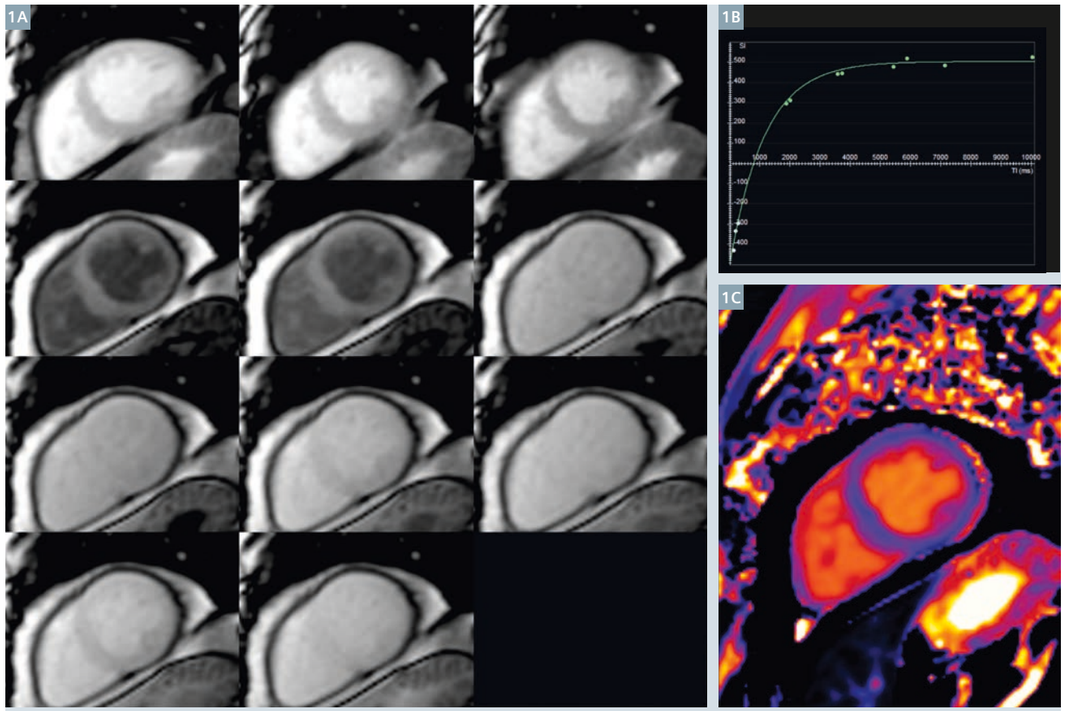

1 MOLLI images **(1A)** with respective signal-time curves **(1B)** and reconstructed T1 map **(1C)** at 3T. The mean T1 time for this patient was 1152 ms (pre-contrast).

Reprinted from MAGNETOM Flash 1/2012

Table 1: Comparison of the MOLLI sequences available for T1 mapping

Sequence	Original MOLLI T1 sequence [15]	Optimized MOLLI sequence [17]	Shortened MOLLI sequence [18]
Preparation	Non-selective inversion recovery	Non-selective inversion recovery	Non-selective inversion recovery
Bandwidth	1090 Hz/px	1090 Hz/px	1090 Hz/px
Flip angle	50°	35°	35°
Base matrix	240	192	192
Phase resolution	151	128	144
FOV × % phase	380 × 342	256 × 100	340 × 75
TI	100 ms	100 ms	100 ms
Slice thickness	8 mm	8 mm	8 mm
Acquisition window	191.1 ms	202 ms	206 ms
Trigger delay	300 ms	300 ms	500 ms
Inversions	3	3	3
Acquisition heartbeats	3,3,5	3,3,5	5,5,1
Recovery heartbeats	3,3,1	3,3,1	1,1,1
TI increment	100–150 ms	80 ms	80 ms
Scan time	17 heartbeats	17 heartbeats	9 heartbeats
Spatial resolution	2.26 × 1.58 × 8 mm	2.1 × 1.8 × 8 mm	1.8 × 1.8 × 8 mm

Reprinted from MAGNETOM Flash 1/2012

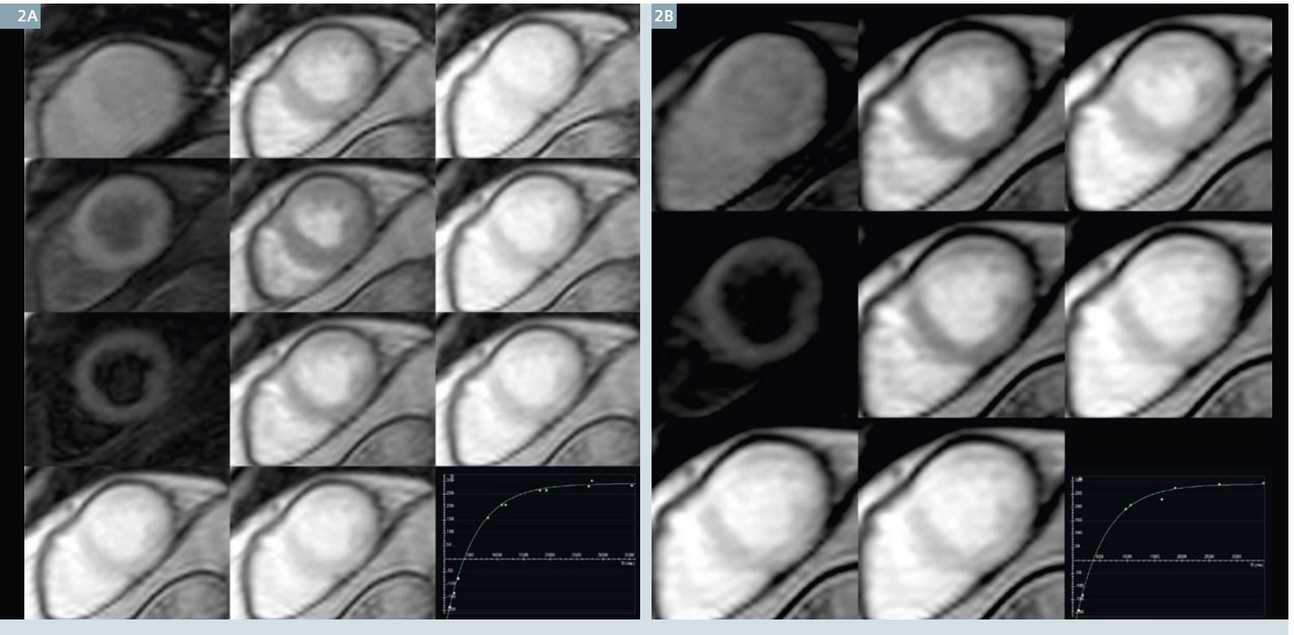

2 MOLLI **(2A)** versus ShMOLLI **(2B)** in a single patient at 3T post-contrast. The calculated values for the 11 MOLLI images were 551 ms versus 544 ms for the 8 images of the shMOLLI set. The time to acquire the MOLLI images were 21 seconds versus 14 seconds for the shMOLLI sequence (with a patient heart rate of 61 bpm).

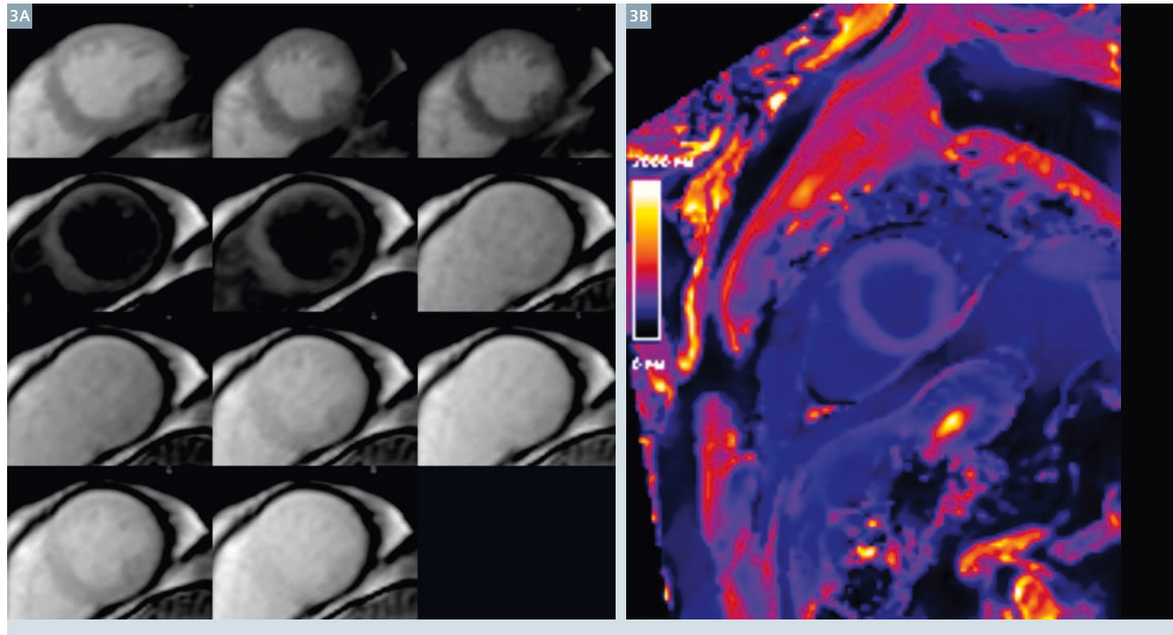

3 An example of an automated T1 map generated on the fly with inline processing after acquisition of a MOLLI sequence at 3T. In **(3A)** the original images acquired and in **(3B)** the inline map. The T1 for this patient was calculated at 525 ms post-contrast.

ing pressure overload, volume overload, aging, oxidative stress and activation of the sympathetic and renin-angiotensin-aldosterone system [5]. Different from replacement fibrosis, where regional collagen deposits appear in areas of myocyte injury, LGE has a limited sensitivity for interstitial diffuse fibrosis [6]. Therefore, if one wants to image diffuse interstitial fibrosis within the myocardium other techniques might be more suitable.

While echocardiogram backscatter and nuclear imaging techniques may be applied for that purpose [7, 8], myocardial tissue characterization is definitely an area where CMR plays a large role. While equilibrium contrast CMR and myocardial tagging have been shown to reflect diffuse myocardial fibrosis, T1 mapping techniques have been most widely used. In the following, we describe the developments in T1 mapping as well as their possible current and future uses.

T1 mapping

By directly quantifying T1 values for each voxel in the myocardium, a parametric map can be generated representing the T1 relaxation times of any region of the heart without the need to compare it to a normal reference standard before or after the use of a contrast agent. The first attempts to measure T1 times in the myocardium used the original Look-Locker sequence and were done using free breathing with acquisition times of over 1 minute per image [9, 10], not allowing for pixel-based-mapping but only for regions-of-interest analysis. Another implementation of T1 mapping used variable sampling of the *k*-space in time (VAST), acquiring images in three to four breath-holds and correlating that data to invasive biopsy [11]. Other sequences have been used for quantification of T1 as well using inversion recovery TrueFISP [12, 13] or multishot saturation recovery images [14] but their reproducibility and accuracy have not been extensively validated.

The most widely used T1 mapping sequence is based on the Modified Look-Locker Inversion-recovery (MOLLI) technique. Described originally by Messroghli et al. [15] it consists of a single shot TrueFISP image with acquisitions over different inversion time readouts allowing for magnetization recovery of a few seconds after 3 to 5 readouts. The parameters for the original MOLLI sequence are described in Table 1. The advantages of this sequence over previous methods are its acquisition in only one relatively short breath-hold, the higher spatial resolution (1.6 × 2.3 × 8 mm) and increased dynamic signal. Reproducibility studies using this sequence have shown that the method is very accurate with a coefficient of variation of 5.4% [16] although an underestimation of 8% should be expected based on phantom data. An example of MOLLI images and its respective signal-time curves and map are shown in Figure 1. One disadvantage of this implementation of MOLLI is its dependence on heart rate, mostly true for T1 values less than 200 msec or greater than 750 msec. However, because the deviation is systematic, raw values can be corrected using the formula $T1_{corrected} = T1_{raw} - (2.7 \times [\text{heart rate } -70])$, bringing the coefficient of variation down to 4.6% after applying the correction. An optimized MOLLI sequence was subsequently described where heart rate correction might not be even necessary [17]. In the optimized sequence, the authors tested variations in readout flip angle, minimum inversion time, inversion time increments and number of pauses between each readout sequence. The conclusion from these experiments showed that a flip angle of 35°, a minimum inversion time of 100 msec, increments of 80 msec and three heart cycle pauses allowed for the most accurate measurement of myocardial T1 (Table 1). Because T1 assessment may be sensitive to motion artifacts and not all patients might be able to hold their breaths throughout all the necessary cardiac cycles used in MOLLI's sequence implementation, more recently a shortened version sequence (ShMOLLI) using only 9 heart beats was presented to account for those limitations [18]. Using incomplete recovery of the longitudinal magnetization that is corrected directly in the scanner by conditional interpretation, ShMOLLI was directly compared to MOLLI in patients over a wide range of T1 times and heart rates both at 1.5 and 3T. The results showed that despite an increase in noise and slight increase in the coefficient of variation (especially at 1.5T), T1 times were not significantly different using ShMOLLI with the advantage of much shorter acquisition times (9.0 ± 1.1 sec versus 17.6 ± 2.9 sec). An example of MOLLI and ShMOLLI images from the same patient is presented in Figure 2.

Up to now, after acquiring images for T1 mapping, one had to analyze them using in-house developed software, dedicated commercial programs or open-source solutions [19], not always a simple and routine task, leading to difficulty in post-processing the data and generating T1 values. Recent advances have provided new inline processing techniques that will generate the T1 maps automatically after image acquisition with MOLLI, without the need for further post-processing, accelerating the whole process. An example of such automated T1 map is presented in Figure 3. At the same time, inline application of motion correction permits more accurate pixel-wise maps, avoiding errors due to respiratory deviations. An example of an image with and without motion correction is presented in Figure 4.

Clinical applications

Potentially, T1 mapping can be used to assess any disease that affects the myocardium promoting diffuse fibrosis. However, because of its recent

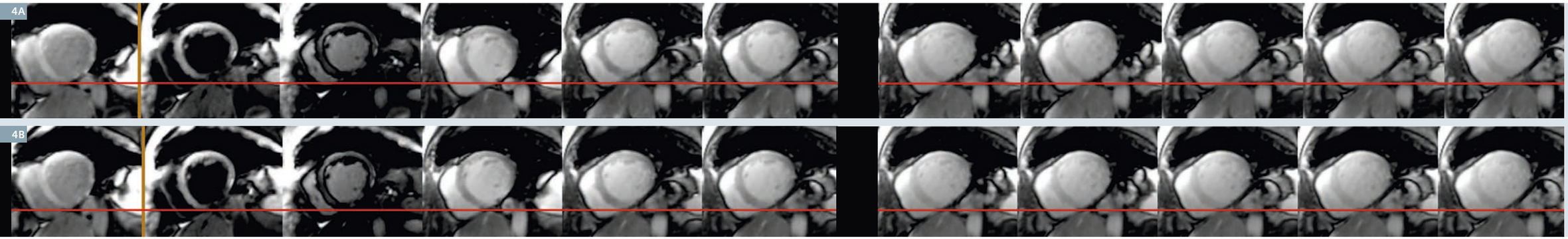

4

Example of a MOLLI sequence obtained without **(4A)** and with **(4B)** motion correction. Notice the deviation from baseline of the left ventricle during the image acquisition cycle, fully corrected in **(4B)**.

development, the technique has only been evaluated on a small number of patients although the clinical scenarios are varied.

The first clinical description of direct T1 mapping in pathological situations was done in patients with acute myocardial infarction [20]. While the authors did not use the described MOLLI sequence, they did note that pre-contrast infarct areas had an 18 ± 7% increase in T1 times compared to normal myocardium and that after contrast the same areas showed a 27 ± 4% reduction compared to non-infarcted areas ($P < 0.05$ for both). In chronic myocardial infarction, where LGE has proven so useful, these changes were also observed although differences were not as pronounced as in the acute setting [21].

In amyloidosis, post-contrast T1 times were also detected to be shorter in the subendocardial regions compared to other myocardium areas [22]. The combination of both LGE identification and T1 times < 191 msec in the subendocardium at 4 minutes provided a 97% concordance in diagnosis of cardiac amyloidosis and T1 values significantly correlated to markers of amyloid load such as left ventricular mass, wall thickness, interatrial thickness and diastolic function.

In valve disease, an attempt to show differences in T1 values in patients with chronic aortic regurgitation using MOLLI sequence did not find any changes in the overall group before or after contrast [23]. However, the authors did notice that differences were observed regionally in segments that demonstrated impaired wall motion in cine images. The small number of patients (n = 8) in the study might have affected the conclusions and further evaluation of similar data might yield other conclusions. A more recent study showed that, using equilibrium contrast CMR, diffuse fibrosis measured in aortic stenosis patients provided significant correlations to quantification on histology [24].

In heart failure, the use of T1 mapping has been more widely studied and directly correlated to histology evaluation [11]. In this paper, the authors evaluated patients with ischemic, idiopathic and restrictive cardiomyopathies showing that post-contrast T1 times at 1.5T were significantly shorter than controls even after exclusion of areas of LGE (429 ± 22 versus 564 ± 23 msec, $P < 0.0001$). We have investigated a similar group of patients on a 3T MAGNETOM Verio scanner and have found that both dilated and hypertrophic cardiomyopathy patients have lower post-contrast T1 times compared to controls, but non-infarcted areas from ischemic cardiomyopathy patients do not show significant differences (unpublished data). Examples of a myocardial T1 map at 3T from a patient with dilated cardiomyopathy and suspected hypertrophic cardiomyopathy are seen in Figure 5 and 6 respectively.

Finally, in patients with both type 1 and 2 diabetes melitus, T1 mapping using CMR was able to show that these patients may have increased interstitial fibrosis compared to controls as T1 times were significantly shorter (425 ± 72 msec versus 504 ± 34 msec, $P < 0.001$) and correlated to global longitudinal strain by echocardiography, demonstrating impaired myocardial systolic function.

Future directions

Certainly with the research of T1 mapping in different clinical scenarios the applicability of the method will increase substantially. In the meantime, more effort has been made to further standardize values across different patients and time points. As T1 time, especially after injection of contrast, depends on both physiologic and scan acquisitions, methods have been described to account for these factors, with normalization of T1 values [25]. More than that, standardization of normal values across a larger number of normal individuals is also necessary since most papers provide data on much reduced cohorts, mostly limited to single center data. In that regard, a large multicenter registry is already collecting data at 3T in patients from 20 to 80 years of age in Latin America [Fernandes JL et al. – www.clinicaltrials.gov – NCT01030549]. Besides that, other techniques are under development that might allow T1 measurement with larger coverage of the heart using 3D methods [26].

Nevertheless, with the current techniques available there are already much more clinical applications to explore and certainly quantitative T1 mapping will become one of the key applications in CMR in the near future.

References

1 Fernandes JL, Pohost GM. Recent advances in cardiovascular magnetic resonance. Rev Cardiovasc Med 2011;12:e107-12.

2 Kim RJ, Wu E, Rafael A, et al. The use of contrast-enhanced magnetic resonance imaging to identify reversible myocardial dysfunction. N Engl J Med 2000;343: 1445-53.

3 Assomull RG, Prasad SK, Lyne J, et al. Cardiovascular magnetic resonance, fibrosis, and prognosis in dilated cardiomyopathy. J Am Coll Cardiol 2006;48: 1977-85.

4 Ordovas KG, Higgins CB. Delayed contrast enhancement on MR images of myocardium: past, present, future. Radiology 2011;261:358-74.

5 Jellis C, Martin J, Narula J, Marwick TH. Assessment of nonischemic myocardial fibrosis. J Am Coll Cardiol 2010;56:89-97.

6 Mewton N, Liu CY, Croisille P, Bluemke D, Lima JA. Assessment of myocardial fibrosis with cardiovascular magnetic resonance. J Am Coll Cardiol 2011;57:891-903.

7 Picano E, Pelosi G, Marzilli M, et al. In vivo quantitative ultrasonic evaluation of myocardial fibrosis in humans. Circulation 1990;81:58-64.

8 van den Borne SW, Isobe S, Verjans JW, et al. Molecular imaging of interstitial alterations in remodeling myocardium after myocardial infarction. J Am Coll Cardiol 2008;52:2017-28.

9 Flacke SJ, Fischer SE, Lorenz CH. Measurement of the gadopentetate dimeglumine partition coefficient in human myocardium in vivo: normal distribution and elevation in acute and chronic infarction. Radiology 2001;218:703-10.

10 Brix G, Schad LR, Deimling M, Lorenz WJ. Fast and precise T1 imaging using a TOMROP sequence. Magn Reson Imaging 1990;8:351-6.

11 Iles L, Pfluger H, Phrommintikul A, et al. Evaluation of diffuse myocardial fibrosis in heart failure with cardiac magnetic resonance contrast-enhanced T1 mapping. J Am Coll Cardiol 2008;52: 1574-80.

12 Schmitt P, Griswold MA, Jakob PM, et al. Inversion recovery TrueFISP: quantification of T(1), T(2), and spin density. Magn Reson Med 2004;51:661-7.

13 Bokacheva L, Huang AJ, Chen Q, et al. Single breath-hold T1 measurement using low flip angle TrueFISP. Magn Reson Med 2006;55:1186-90.

14 Wacker CM, Bock M, Hartlep AW, et al. Changes in myocardial oxygenation and perfusion under pharmacological stress with dipyridamole: assessment using T*2 and T1 measurements. Magn Reson Med 1999;41:686-95.

15 Messroghli DR, Radjenovic A, Kozerke S, Higgins DM, Sivananthan MU, Ridgway JP. Modified Look-Locker inversion recovery (MOLLI) for high-resolution T1 mapping of the heart. Magn Reson Med 2004;52: 141-6.

16 Messroghli DR, Plein S, Higgins DM, et al. Human myocardium: single-breath-hold MR T1 mapping with high spatial resolution--reproducibility study. Radiology 2006;238:1004-12.

17 Messroghli DR, Greiser A, Frohlich M, Dietz R, Schulz-Menger J. Optimization and validation of a fully-integrated pulse sequence for modified look-locker inversion-recovery (MOLLI) T1 mapping of the heart. J Magn Reson Imaging 2007;26:1081-6.

18 Piechnik SK, Ferreira VM, Dall'Armellina E, et al. Shortened Modified Look-Locker Inversion recovery (ShMOLLI) for clinical myocardial T1 mapping at 1.5 and 3 T within a 9 heartbeat breathhold. J Cardiovasc Magn Reson 2010;12:69.

19 Messroghli DR, Rudolph A, Abdel-Aty H, et al. An open-source software tool for the generation of relaxation time maps in magnetic resonance imaging. BMC Med Imaging 2010; 10:16.

20 Messroghli DR, Niendorf T, Schulz-Menger J, Dietz R, Friedrich MG. T1 mapping in patients with acute myocardial infarction. J Cardiovasc Magn Reson 2003;5:353-9.

21 Messroghli DR, Walters K, Plein S, et al. Myocardial T1 mapping: application to patients with acute and chronic myocardial infarction. Magn Reson Med 2007;58:34-40.

22 Maceira AM, Joshi J, Prasad SK, et al. Cardiovascular magnetic resonance in cardiac amyloidosis. Circulation 2005;111:186-93.

23 Sparrow P, Messroghli DR, Reid S, Ridgway JP, Bainbridge G, Sivananthan MU. Myocardial T1 mapping for detection of left ventricular myocardial fibrosis in chronic aortic regurgitation: pilot study. AJR Am J Roentgenol 2006;187:W630-5.

24 Flett AS, Hayward MP, Ashworth MT, et al. Equilibrium contrast cardiovascular magnetic resonance for the measurement of diffuse myocardial fibrosis: preliminary validation in humans. Circulation 2010; 122:138-44.

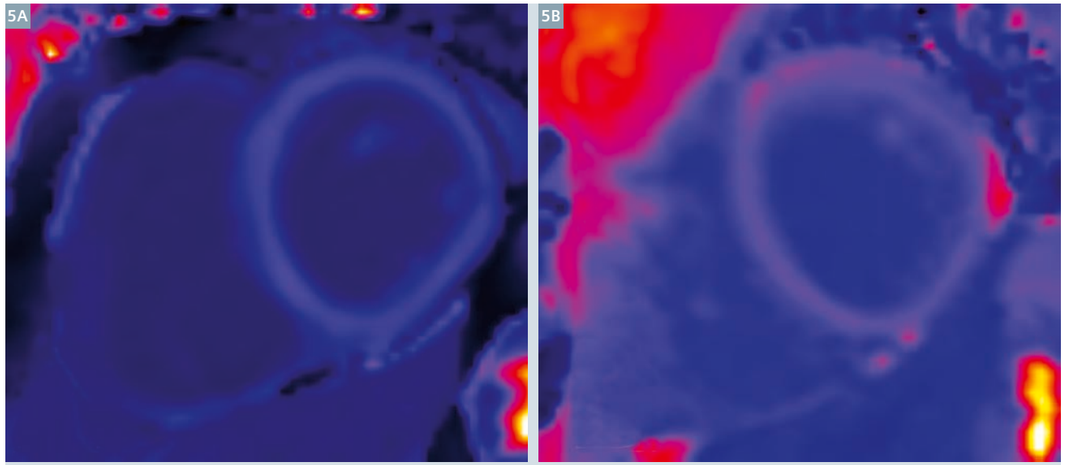

5 T1 mapping at 3T after contrast of a patient with **(5A)** dilated cardiomyopathy (T1 of 507 ms) in comparison to **(5B)** a control patient (T1 of 615 ms).

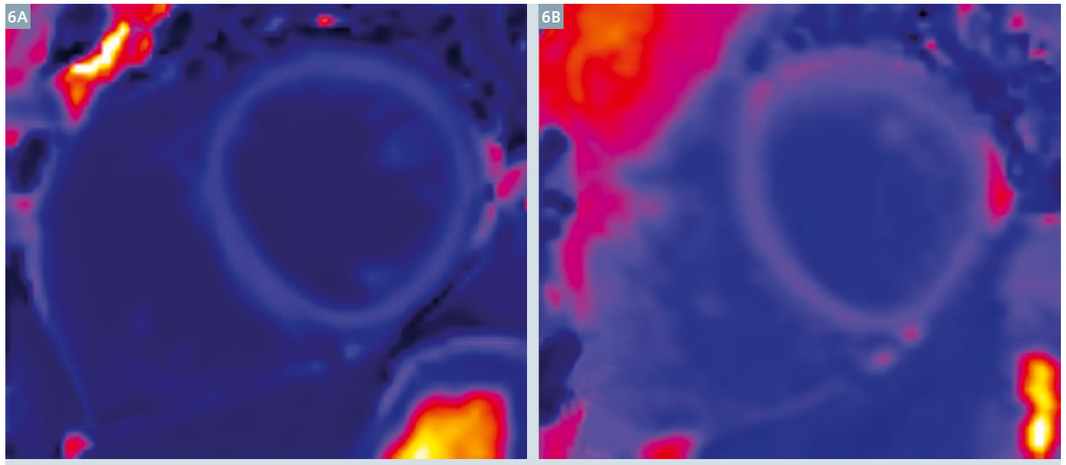

6 T1 mapping of a patient with **(6A)** suspected hypertrophic cardiomyopathy (T1 of 466 ms) in comparison to **(6B)** a control patient (with a T1 of 615 ms).

25 Gai N, Turkbey EB, Nazarian S, et al. T1 mapping of the gadolinium-enhanced myocardium: adjustment for factors affecting interpatient comparison. Magn Reson Med 2011;65:1407-15.
26 Coolen BF, Geelen T, Paulis LE, Nauerth A, Nicolay K, Strijkers GJ. Three-dimensional T1 mapping of the mouse heart using variable flip angle steady-state MR imaging. NMR Biomed 2011;24:154-62.

Contact

Juliano L Fernandes
R. Antonio Lapa 1032
Campinas-SP – 13025-292
Brazil
Phone: +55-19-3579-2903
Fax: +55-19-3252-2903
jlaraf@fcm.unicamp.br

Reprinted from MAGNETOM Flash 1/2012

Preliminary Experiences with Compressed Sensing Multi-Slice Cine Acquisitions for the Assessment of Left Ventricular Function: CV_sparse WIP

G. Vincenti, M.D.[1]; D. Piccini[2,4]; P. Monney, M.D.[1]; J. Chaptinel[3]; T. Rutz, M.D.[1]; S. Coppo[3]; M. O. Zenge, Ph.D.[4]; M. Schmidt[4]; M. S. Nadar[5]; Q. Wang[5]; P. Chevre[1, 6]; M.; Stuber, Ph.D.[3]; J. Schwitter, M.D.[1]

[1]Division of Cardiology and Cardiac MR Center, University Hospital of Lausanne (CHUV), Lausanne, Switzerland
[2]Advanced Clinical Imaging Technology, Siemens Healthcare IM BM PI, Lausanne, Switzerland
[3]Department of Radiology, University Hospital (CHUV) and University of Lausanne (UNIL) / Center for Biomedical Imaging (CIBM), Lausanne, Switzerland
[4]MR Applications and Workflow Development, Healthcare Sector, Siemens AG, Erlangen, Germany
[5]Siemens Corportate Technology, Princeton, USA
[6]Department of Radiology, University Hospital Lausanne, Switzerland

Introduction

Left ventricular (LV) ejection fraction is one of the most important measures in cardiology and part of every cardiac imaging evaluation as it is recognized as one of the strongest predictors of outcome [1]. It allows to assess the effect of established or novel treatments [2], and it is crucial for decision making [3] e.g. to start [4] or stop [5] specific drug treatments or to implant devices [6]. CMR is generally accepted as the gold standard method to yield most accurate measures of LV ejection fraction and LV volumes. This capability and the additional value of CMR to characterize pathological myocardial tissue was the basis to assign a class 1 indication for patients with known or suspected heart failure to undergo CMR in the new Heart Failure Guidelines of the European Society of Cardiology [3].

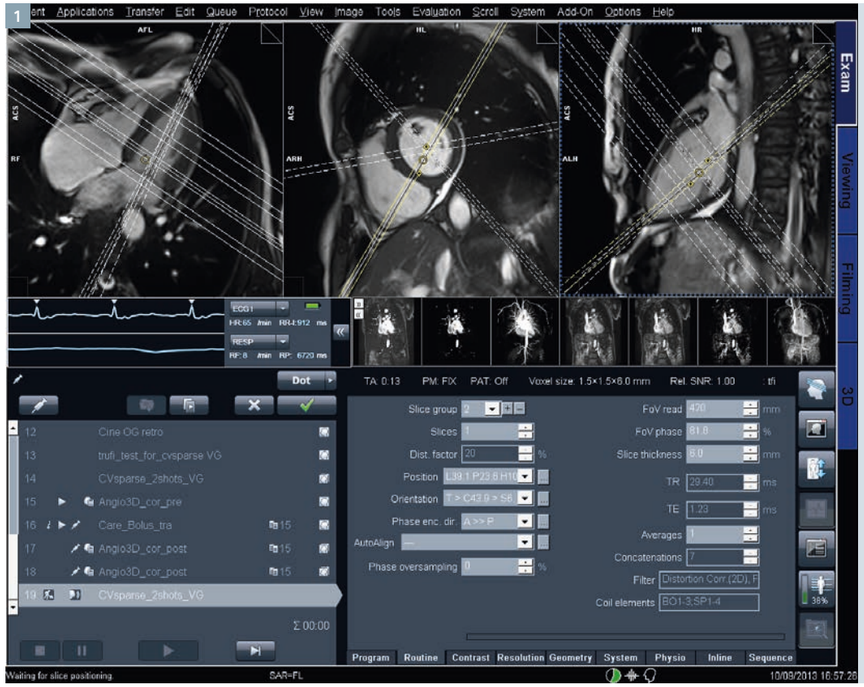

1 Display of the planning of the 7 slices (4 short axis and 3 long axis slices) acquired within a single breath-hold with the three localizers.

The evaluation of LV volumes and LV ejection fraction are based on well-defined protocols [7] and it involves the acquisition of a stack of LV short axis cine images from which volumes are calculated by applying Simpson's rule. These stacks are typically acquired in multiple breath-holds. Quality criteria [8] for these functional images are available and are implemented e.g. for the quality assessment within the European CMR registry which currently holds approximately 33,000 patients and connects 59 centers [9].

Recently, compressed sensing (CS) techniques emerged as a means to considerably accelerate data acquisition without compromising significantly image quality. CS has three requirements:

1) transform sparsity,
2) incoherence of undersampling artifacts, and
3) nonlinear reconstruction (for details, see below).

Based on these prerequisites, a CS approach for the acquisition of cardiac cine images was developed and tested*. In particular, the potential to acquire several slices covering the heart in different orientations within a single breath-hold would allow to apply model-based analysis tools which theoretically could improve the motion assessment at the base of the heart, where considerable through-plane motion on short-axis slices can introduce substantial errors in LV volume and LV ejection fraction calculations. Conversely, with a multi-breath-hold approach, there are typically small differences in breath-hold positions which can introduce errors in volume and function calculations. The pulse sequence tested here allows for the acquisition of 7 cine slices within 14 heartbeats with an excellent temporal and spatial resolution.

*Work in progress: The product is still under development and not commercially available yet. Its future availability cannot be ensured.

Such a pulse sequence would also offer the advantage to obtain functional information in at least a single plane in patients unable to hold their breath for several heartbeats or in patients with frequent extrasystoles or atrial fibrillation. However, it should be mentioned that accurate quantitative measures of LV volumes and function cannot be obtained in highly arrhythmic hearts or in atrial fibrillation, as under such conditions volumes and ejection fraction change from beat to beat due to variable filling conditions. Nevertheless, rough estimates of LV volumes and function would still be desirable in arrhythmic patients.

In a group of healthy volunteers and patients with different LV pathologies, the novel single-breath-hold CS cine approach was compared with the standard multi-breath-hold cine technique with respect to measure LV volumes and LV ejection fraction.

The CV_sparse work-in-progress (WIP)

The CV_sparse WIP package implements sparse, incoherent sampling and iterative reconstruction for cardiac applications. This method in principle allows for high acceleration factors which enable triggered 2D real-time cine CMR while preserving high spatial and/or temporal resolution of conventional cine acquisitions. Compressed sensing methods exploit the potential of image compression during the acquisition of raw input data. Three components [10] are crucial for the concept of compressed sensing to work

I. Sparsity: In order to guarantee compressibility of the input data, sparsity must be present in a specific transform domain. Sparsity can be computed e.g. by calculating differences between neighboring pixels or by calculating finite differences in angiograms which then detect primarily vessel contours which typically represent a few percent of the

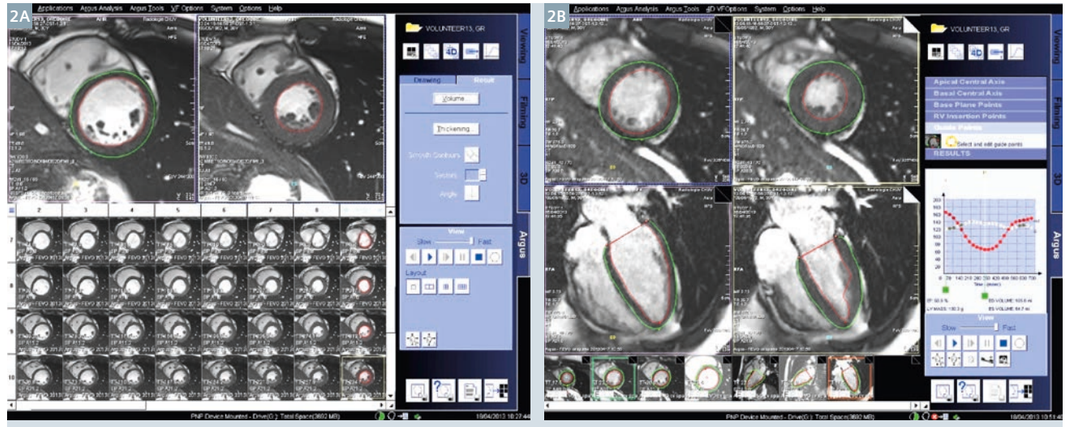

2 Displays of the data analysis tools for the conventional short axis stack of cine images covering the entire LV **(2A)** and the 4D analysis tool **(2B)**, which is model-based and takes long axis shortening of the LV, i.e. mitral annulus motion into account. Note that with both analysis tools, LV trabeculations are included into the LV volume, particularly in the end-diastolic images (corresponding images on the left of top row in 2A and 2B).

3

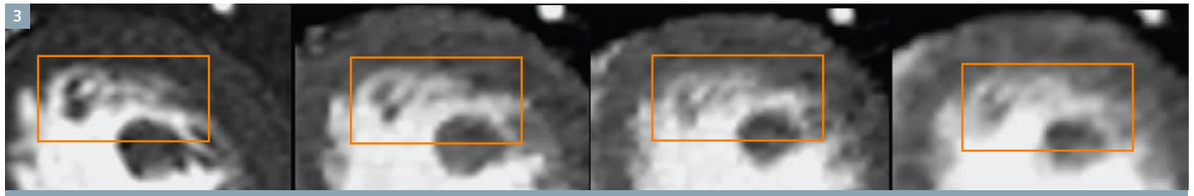

3 Examples of visualization of small trabecular structures in the LV (in the rectangle) with the standard cine SSFP sequence (image on the left) and the accelerated compressed sensing sequences (images on the right). Despite increasing acceleration most information on small intraluminal structures remains visible.

entire image data only. Furthermore, sparsity is not limited to the spatial domain: the acquisition of cine images of the heart can be highly sparsified in the temporal dimension.

II. Incoherent sampling: The aliasing artifacts due to *k*-space undersampling must be incoherent, i.e. noise-like, in that transform domain. Here, it is to mention that fully random *k*-space sampling is suboptimal as *k*-space trajectories should be smooth for hardware and physiological considerations. Therefore, incoherent sampling schemes must be designed to avoid these concerns while fulfilling the condition of random, i.e. incoherent sampling.

III. Reconstruction: A non-linear iterative optimization corrects for subsampling artifacts during the process of image reconstruction yielding to a best solution with a sparse representation in a specific transform domain and which is consistent with the input data. Such compressed sensing techniques can also be combined with parallel imaging techniques [11].

WIP CV_sparse Sequence

The current CV_sparse sequence [12] realizes incoherent sampling by initially distributing the readouts pseudo-randomly on the Cartesian grid in *k*-space. In addition, for cine-CMR imaging, a pseudo-random offset is applied from frame-to-frame which results in an incoherent temporal jitter. Finally, a variable sampling density in *k*-space stabilizes the iterative reconstruction. To avoid eddy current effects for balanced steady-state free precession (bSSFP) acquisitions, pairing [13] can also be applied. Thus, the tested CV_sparse sequence is characterized by sparse, incoherent sampling in space and time, non-linear iterative reconstruction integrating SENSE, and L1 wavelet regularization in the phase encoding direction and/or the temporal dimension. With regard to reconstruction, the ICE program runs a non-linear iterative reconstruction with *k-t* regularization in space and time specifically modified for compressed sensing. The algorithm derives from a parallel imaging type reconstruction which takes coil sensitivity maps into account, thus supporting predominantly high acceleration factors. For cine CMR, no additional reference scans are needed because – similar to TPAT – the coil sensitivity maps are calculated from the temporal average of the input data in a central region of *k*-space consisting of not more than 48 reference lines. The extensive calculations for image reconstruction typically running 80 iterations are performed online on all CPUs on the MARS computer in parallel, in order to reduce reconstruction times.

Volunteer and Patient studies

In order to obtain insight into the image quality of single-breath-hold multi-slice cine CMR images acquired with the compressed sensing (CS) approach, we studied a group of healthy volunteers and a patient group with different pathologies of the left ventricle. In addition to the evaluation of image quality, the robustness and the precision of the CS approach for LV volumes and LV ejection fraction was also assessed in comparison with a standard high-resolution cine CMR approach. All CMR examinations were performed on a 1.5T MAGNETOM Aera (Siemens Healthcare, Erlangen, Germany). The imaging protocol consisted of a set of cardiac localizers followed by the acquisition of a stack of conventional short-axis SSFP cine images covering the entire LV with a spatial and temporal resolution of 1.2 x 1.6 mm², and approximately 40 ms, respectively (slice thickness: 8 mm; gap between slices: 2 mm). LV 2-chamber, 3-chamber, and 4-chamber long-axis acquisitions were obtained for image quality assessment but were not used for LV volume quantifications. As a next step, to test the new CS-based technique, slice orientations were planned to cover the LV with 4 short-axis slices distributed evenly over the LV long axis complemented by 3 long-axis slices (i.e. a 2-chamber, 3-chamber, and 4-chamber slice) (Fig. 1). These 7 slices were then acquired in a single breath-hold maneuver lasting 14 heart beats (i.e. 2 heart beats per slice) resulting in an acceleration factor of 11.0 with a temporal and spatial resolution of 30 ms and 1.5 x 1.5 mm², respectively (slice thickness: 6 mm). As the reconstruction algorithm is susceptible to aliasing in the phase-encoding direction, the 7 slices were first acquired with a non-cine acquisition to check for correct phase-encoding directions and, if needed, to adjust the field-of-view to avoid fold-over artifacts. After confirmation of correct imaging parameters, the 7-slice single-breath-hold cine CS-acquisition was performed. In order to obtain a reference for the LV volume measurement, a phase-contrast flow measurement in the ascending aorta was performed to be compared with the LV stroke volumes calculated from the standard and CS cine data.

The conventional stack of cine SSFP images was analyzed by the Argus software (Siemens Argus 4D Ventricular Function, Fig. 2A). The CS cine data were analyzed by the 4D-Argus software (Siemens Argus, Fig. 2B). Such software is based on an LV model and, with relatively few operator interactions, the contours for the LV endocardium and epicardium are generated by the analysis tool. Of note, this 4D analysis tool automatically tracks the 3-dimensional motion of the mitral annulus throughout the cardiac cycle which allows for an accurate volume calculation particularly at the base of the heart.

4

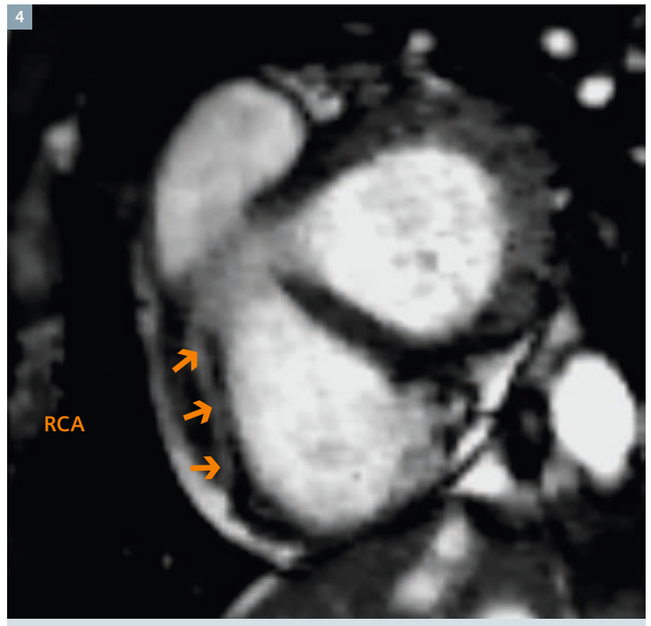

4 Example demonstrating the performance of the compressed sensing technique visualizing small structures such as the right coronary artery (RCA) with high temporal and spatial resolution acquired within 2 heartbeats. Short-axis view of the base of the heart (1 out of 17 frames).

Results and discussion
Image quality – robustness of the technique

Overall, a very good image quality of the single-breath-hold multi-slice CS acquisitions was obtained in the 12 volunteers and 14 patient studies. All CS data sets were of adequate quality to undergo 4D analysis. Small structures such as trabeculations were visualized in the CS data sets as shown in Figures 3 and 4. However, very small structures, detectable by the conventional cine acquisitions, were less well discernible by the CS images. Therefore, it should be mentioned here, that this accelerated single-breath-hold CS approach would be adequate for functional measurements, i.e. LV ejection fraction assessment (see also results below), whereas assessment of small structures as present in many cardiomyopathies is more reliable when performed on conventional cine images. Temporal resolution of the new technique appears adequate to even detect visually the dyssynchroneous contraction pattern in left bundle branch block. Also, the image contrast between the LV myocardium and the blood pool was high on the CS images allowing for an easy assessment of the LV motion pattern. As a result, the single-breath-hold cine approach permits to reconstruct the LV in 3D space with high temporal resolution as illustrated in Figure 5. Since these data allow to correctly include the 3D motion of the base of the heart during the cardiac cycle, the LV stroke volume appears to be measurable by the CS approach with higher accuracy than with the conventional multi-breath-hold approach (see results below). With an accurate measurement of the LV stroke volume, the quantification of a mitral insufficiency should theoretically benefit (when calculating mitral regurgitant volume as 'LV stroke volume minus aortic forward-flow volume').

As a current limitation of the CS approach, its susceptibility for fold-over artifacts should be mentioned (Figs. 6A). Therefore, the field-of-view must cover the entire anatomy and thus, some penalty in spatial res-

olution may occur in relation to the patient's anatomy. In addition, the sparsity in the temporal domain may be limited in anatomical regions of very high flow, and therefore, in some acquisitions, flow-related artifacts occurred in the phase-encoding direction during systole (Figs. 6B, C). Also, in its current version, the sequence is prospective, thus it does not cover the very last phases of the cardiac cycle and the reconstruction times for the CS images lasted several minutes precluding an immediate assessment of the image data quality or using this image information to plan next steps of a CMR examination.

Performance of the single-breath-hold CS approach in comparison with the standard multi-breath-hold cine approach

From a quantitative point-of-view, the accurate and reliable measurement of LV volumes and function is crucial as many therapeutic decisions directly depend on these measures [3–6]. In this current relatively small study group, LV end-diastolic and end-systolic volumes measured by the single-breath-hold CS approach were comparable with those calculated from the standard multi-breath-hold cine SSFP approach. LVEDV and LVESV differed by 10 ml ± 17 ml and 2 ml ± 12 ml, respectively. Most importantly, LV ejection fraction differed by only 1.3 ± 4.7% (50.6% vs 49.3% for multi-breath-hold and single-breath-hold, respectively, $p = 0.17$; regression: $r = 0.96$, $p < 0.0001$; $y = 0.96x + 0.8$ ml). Thus, it can be concluded that the single-breath-hold CS approach could potentially replace the multi-breath-hold standard technique for the assessment of LV volumes and systolic function.

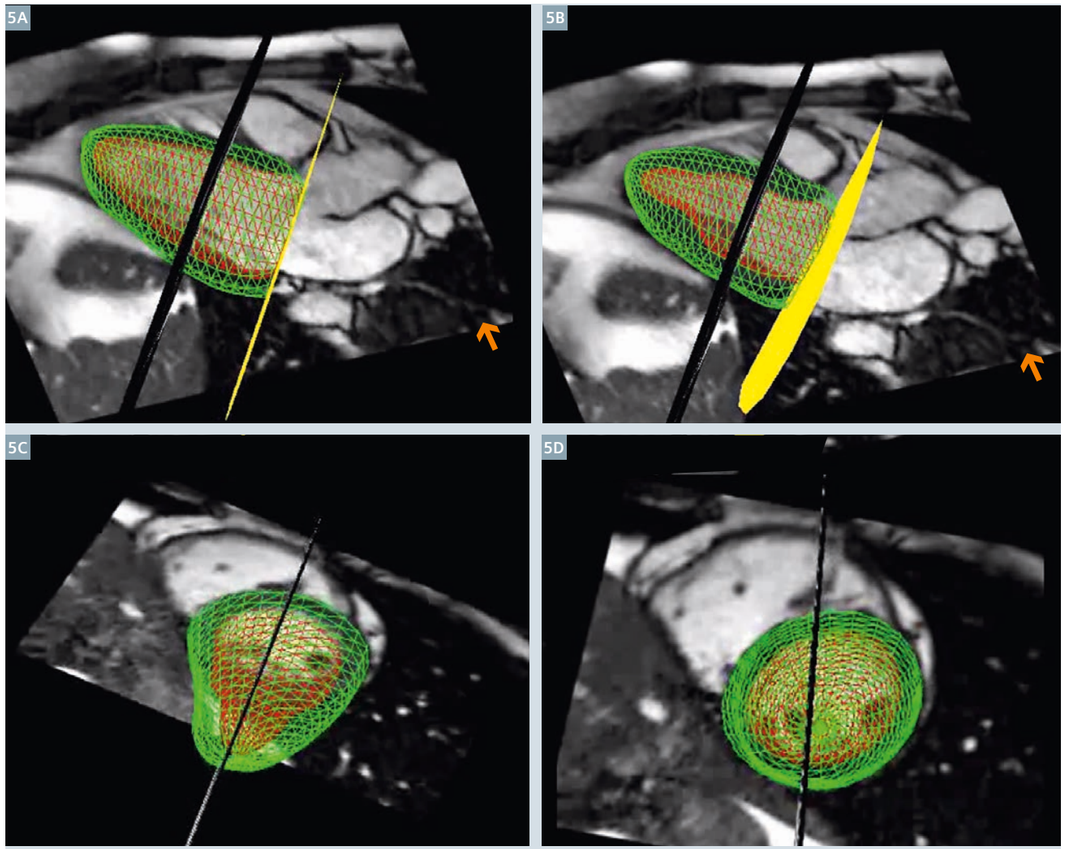

5 Display of the 3D reconstruction derived from the 7 slices acquired within a single breath-hold. Note the long-axis shortening of the LV during systole allowing for accurate LV volume measurements (**5A, 5B**, yellow plane). Any orientation of the 3D is available for inspection of function **(5A–D)**.

Reprinted from MAGNETOM Flash 5/2013

What about the accuracy of the novel single-breath-hold CS technique?

To assess the accuracy of the LV volume measurements, LV stroke volume was compared with the LV output measured in the ascending aorta with phase-contrast MR. As the flow measurements were performed distally to the coronary arteries, flow in the coronaries was estimated as the LV mass multiplied by 0.8 ml/min/g. An excellent agreement was found with a mean of 86.8 ml/beat for the aortic flow measurement and 91.9 ml/beat for the LV measurements derived from the single-breath-hold CS data ($r = 0.93$, $p < 0.0001$). By Bland-Altman analysis, the stroke volume approach overestimated by 5.2 ml/beat versus the reference flow measurement. For the conventional stroke volume measurements, this difference was 15.6 ml/beat (linear regression analysis vs aortic flow: $r = 0.69$, $p < 0.01$). More importantly, the CS LV stroke data were not only more precise with a smaller mean difference, the variability of the CS data vs the reference flow data was less with a standard deviation as low as 6.8 ml/beat vs 12.9 ml/beat for the standard multi-breath-hold approach (Fig. 7). Several explanations may apply for the higher accuracy of the single-breath-hold multi-slice CS approach in comparison to the conventional multi-breath-hold approach:

1) With the single-breath-hold approach, all acquired slices are correctly co-registered, i.e. they are correctly aligned in space, a prerequisite for the 4D-analysis tool to work properly.

2) This 4D-analysis tool allows for an accurate tracking of the mitral valve plane motion during the cardiac cycle as shown in Figure 5, which is important as the cross-sectional area of the heart at its base is large and thus, inaccurate slice positioning at the base of

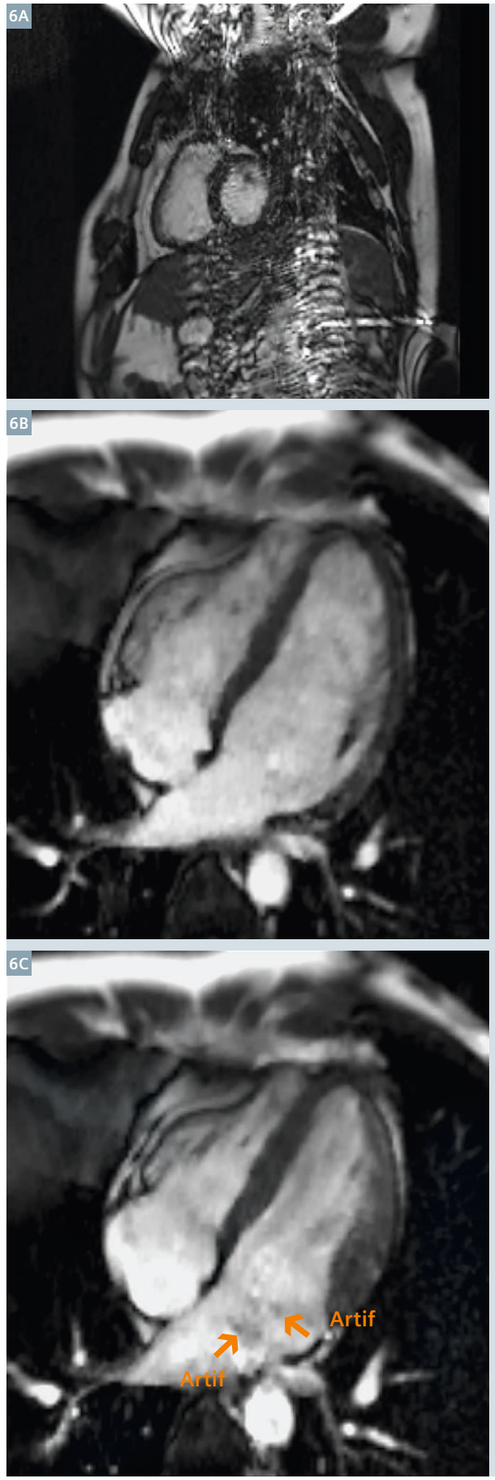

6A A typical fold-over artifact along the phase-encoding direction in a short axis slice, oriented superior-inferior for demonstrative purpose.

6B No flow-related artifacts are visible on the end-diastolic phases, while small artifacts in phase-encoding direction (Artif, arrows) occur in mid-systole projecting over the mitral valve **(6C).**

Reprinted from MAGNETOM Flash 5/2013

7

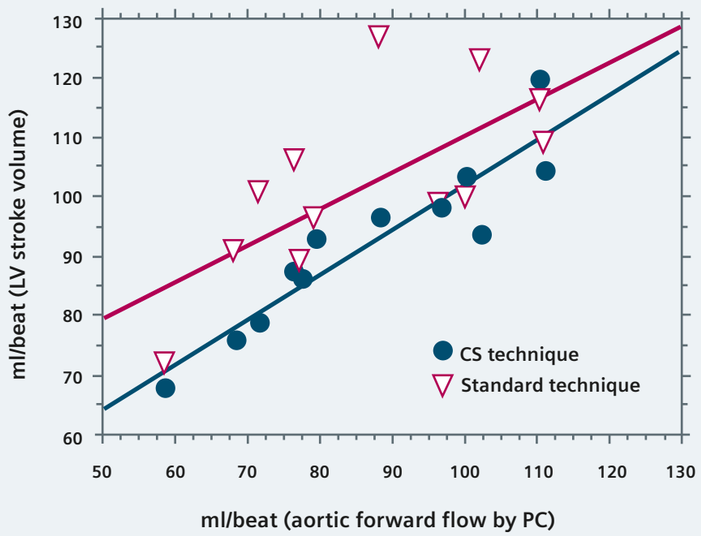

7 An excellent correlation is obtained for the LV stroke volume calculated from the compressed sensing data with the flow volume in the aorta measured by phase-contast technique. Variability of the conventional LV stroke volume data appears higher than for the compressed sensing data.

the heart with conventional short-axis slices typically translate in relatively large errors. Nevertheless, we observed a systematic overestimation of the stroke volume by the CS approach of 5.2 ml/beat in comparison to the flow measurements. In normal hearts with tricuspid aortic valves, an underestimation of aortic flow by the phase-contrast technique is very unlikely [14]. Thus, overestimation of stroke volume by the volume approach is to consider. In the volume contours, the papillary muscles are excluded as illustrated in Figure 8. As these papillary muscles are excluded in both the diastolic and systolic contours, this aspect should not affect net LV stroke volume. However, as shown in Figure 8, smaller trabeculations of the LV wall are included into the LV blood pool contour in the diastolic phase, while these trabeculations, when compacted in the end-systolic phase, are excluded from the blood pool resulting in a small overestimation of the end-diastolic volume, and thus, LV stroke volume. This explanation is likely as Van Rossum et al. demonstrated a slight underestimation of the LV mass when calculated on end-diastolic phases versus end-systolic phases, as trabeculations in end-diastole are typically excluded from the LV walls [15].

In summary, this novel very fast acquisition strategy based on a CS technique allows to cover the entire LV with high temporal and spatial resolution within a single breath-hold. The image quality based on these preliminary results appears adequate to yield highly accurate measures of LV volumes, LV stroke volume, LV mass, and LV ejection fraction. Testing of this very fast multi-slice cine approach for the atria and the right ventricle is currently ongoing. Finally, these preliminary data show that compressed sensing MR acquisitions in the heart are feasible in humans and compressed sensing might be implemented for other important cardiac sequences such as fibrosis/viability imaging, i.e. late gadolinium enhancement, coronary MR angiography, or MR first-pass perfusion.

The Cardiac MR Center of the University Hospital Lausanne

The Cardiac Magnetic Resonance Center (CRMC) of the University Hospital of Lausanne (Centre Hospitalier Universitaire Vaudois; CHUV) was established in 2009. The CMR center is dedicated to high-quality clinical work-up of cardiac patients, to deliver state-of-the-art training in CMR to cardiologists and radiologists, and to pursue research. In the CMR center education is provided for two specialties while focusing on one organ system. Traditionally, radiologists have focussed on using one technique for different organs, while cardiologists have concentrated on one organ and perhaps one technique. Now in the CMR center the focus is put on a combination of specialists with different background on one organ. Research at the CMR center is devoted to four major areas: the study of

1.) cardiac function and tissue characterization, specifically to better understand diastolic dysfunction,
2.) the development of MR-compatible cardiac devices such as pacemakers and ICDs;
3.) the utilization of hyperpolarized ^{13}C-carbon contrast media to investigate metabolism in the heart, and
4.) the development of ^{19}F-fluorine-based CMR techniques to detect inflammation and to label and track cells non-invasively.

For the latter two topics, the CMR center established tight collaborations with the Center for Biomedical Imaging (CIBM), a network around Lake Geneva that includes the Ecole Polytechnique Fédérale de Lausanne (EPFL), and the universities and university hospitals of Lausanne and Geneva. In particular, strong collaborative links are in place with the CVMR team of Prof. Matthias Stuber, a part of the CIBM and located at the University Hospital Lausanne and with Prof. A. Comment, with whom we perform the studies on real-time metabolism based on the ^{13}C-carbon hyperpolarization (DNP) technique. In addition, collaborative studies are ongoing with the Heart Failure and Cardiac Transplantation Unit led by Prof. R. Hullin (detection of graft rejection by tissue characterization) and the Oncology Department led by Prof. Coukos (T cell tracking by ^{19}F-MRI in collaboration with Prof. Stuber, R. van Heeswijk, CIBM, and Prof. O. Michielin, Oncology). This structure allows for a direct interdisciplinary interaction between physicians, engineers, and basic scientists on a daily basis with the aim to enable innovative research and fast translation of these techniques from bench to bedside.

The CMRC is also the center of competence for the quality assessment of the European CMR registry which holds currently approximately 33,000 patient studies acquired in 59 centers across Europe.

The members of the CRMC team are: Prof. J. Schwitter (director of the center), PD Dr. X. Jeanrenaud, Dr. D. Locca, MER, Dr. P. Monney, Dr. T. Rutz, Dr. C. Sierro, and Dr. S. Koestner (cardiologists, staff members),

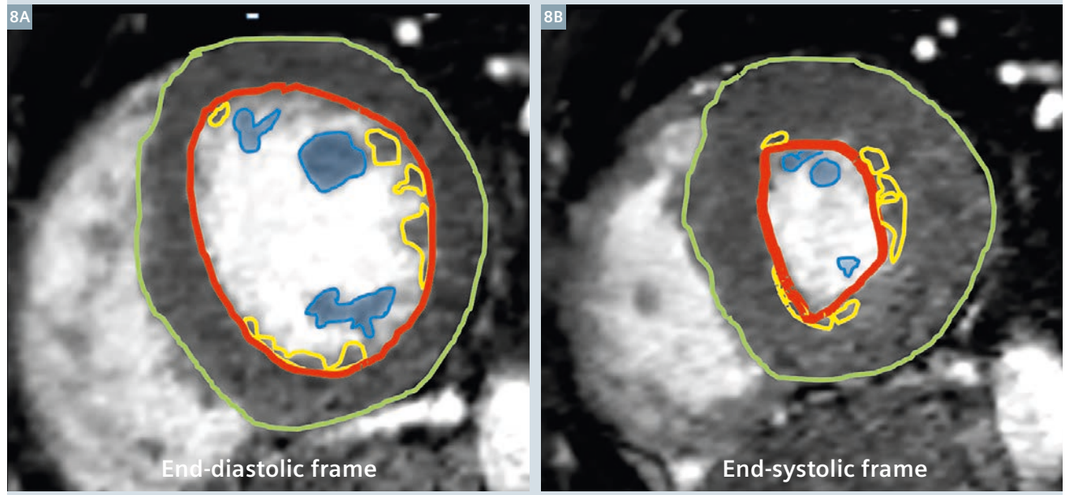

8 Overestimation of end-diastolic LV volumes by volumetric measurements. In comparison to ejected blood from the LV as measured with phase-contrast techniques, the volumetric measurements of LV stroke volume overestimated by approximately 5 ml, most likely by overestimation of LV end-diastolic volume. Small trabculations (yellow contours in 8A) are included into the LV blood volume (red contour in 8A) in diastole, while these trabeculations (yellow contours in 8B) are typically included in the end-systolic phase (red contours in 8B). For the same reasons, LV mass (= green contour minus red contour) is often slightly underestimated in diastole vs systole.

Dr. G. Vincenti (cardiologist) and Dr. N. Barras (cardiologist in training, rotation), PD. Dr. S. Muzzarellli (affiliated cardiologist), Prof. C. Beigelman and Dr. X. Boulanger (radiologists, staff members), Dr. G.L. Fetz (radiologist in training, rotation), C. Gonzales, PhD (^{19}F-fluorine project leader), H. Yoshihara, PhD (^{13}C-carbon project leader), V. Klinke (medical student, doctoral thesis), C. Bongard (medical student, master thesis), P. Chevre (chief CMR technician), and F. Recordon and N. Lauriers (research nurses).

Acknowledgements

The authors would like to thank all the members of the team of MR technologists at the CHUV for their highly valuable participation, helpfulness and support during the daily clinical CMR examinations and with the research protocols. Finally, a very important acknowledgment goes to Dr. Michael Zenge, Ms. Michaela Schmidt, and the whole Siemens MR Cardio team of Edgar Müller in Erlangen.

References

1 Curtis JP, Sokol SI, Wang Y, Rathore SS, Ko DT, Jadbabaie F, Portnay EL, Marshalko SJ, Radford MJ, Krumholz HM. The association of left ventricular ejection fraction, mortality, and cause of death in stable outpatients with heart failure. Journal of the American College of Cardiology. 2003;42(4):736-42.

2 Sürder D, Manka R, Lo Cicero V, Moccetti T, Rufibach K, Soncin S, Turchetto L, Radrizzani M, Astori G, Schwitter J, Erne P, Jamshidi P, Auf Der Maur C, Zuber M, Windecker S, Moschovitis A, Wahl A, Bühler I, Wyss C, Landmesser U, Lüscher T, Corti R. Intracoronary injection of bone marrow derived mononuclear cells, early or late after acute myocardial infarction: Effects on global LV-function: 4 months results of the SWISS-AMI trial. Circulation. 2013;127:1968-79.

3 McMurray JJV, Adamopoulos S, Anker SD, Auricchio A, Böhm M, Dickstein K, Falk V, Filippatos G, Fonseca C, Sanchez MAG, Jaarsma T, Køber L, Lip GYH, Maggioni AP, Parkhomenko A, Pieske BM, Popescu BA, Rønnevik PK, Rutten FH, Schwitter J, Seferovic P, Stepinska J, Trindade PT, Voors AA, Zannad F, Zeiher A. ESC Guidelines for the diagnosis and treatment of acute and chronic heart failure 2012. European Heart Journal. 2012 May 19, 2012(33):1787–847.

4 Zannad F, McMurray JJV, Krum H, van Veldhuisen DJ, Swedberg K, Shi H, Vincent J, Pocock SJ, Pitt B. Eplerenone in Patients with Systolic Heart Failure and Mild Symptoms. New England Journal of Medicine. 2011;364(1):11-21.

5 Gharib MI, Burnett AK. Chemotherapy-induced cardiotoxicity: current practice and prospects of prophylaxis. European Journal of Heart Failure. 2002 June 1, 2002;4(3):235-42.

6 Bardy GH, Lee KL, Mark DB, Poole JE, Packer DL, Boineau R, Domanski M, Troutman C, Anderson J, Johnson G, McNulty SE, Clapp-Channing N, Davidson-Ray LD, Fraulo ES, Fishbein DP, Luceri RM, Ip JH. Amiodarone or an Implantable Cardioverter–Defibrillator for Congestive Heart Failure. New England Journal of Medicine. 2005;352(3):225-37.

7 Schwitter J. CMR-Update. 2. Edition ed. Lausanne, Switzerland. www.herz-mri.ch.

8 Klinke V, Muzzarelli S, Lauriers N, Locca D, Vincenti G, Monney P, Lu C, Nothnagel D, Pilz G, Lombardi M, van Rossum A, Wagner A, Bruder O, Mahrholdt H, Schwitter J. Quality assessment of cardiovascular magnetic resonance in the setting of the European CMR registry: description and validation of standardized criteria. Journal of Cardiovascular Magnetic Resonance. 2013;15(1):55.

9 Bruder O, Wagner A, Lombardi M, Schwitter J, van Rossum A, Pilz G, Nothnagel D, Steen H, Petersen S, Nagel E, Prasad S, Schumm J, Greulich S, Cagnolo A, Monney P, Deluigi C, Dill T, Frank H, Sabin G, Schneider S, Mahrholdt H. European Cardiovascular Magnetic Resonance (EuroCMR) registry-multi national results from 57 centers in 15 countries. J Cardiovasc Magn Reson. 2013;15:1-9.

10 Lustig M, Donoho D, Pauly JM. Sparse MRI: The application of compressed sensing for rapid MR imaging. Magnetic Resonance in Medicine. 2007;58(6):1182-95.

11 Liang D, Liu B, Wang J, Ying L. Accelerating SENSE using compressed sensing. Magnetic Resonance in Medicine. 2009;62(6): 1574-84.

12 Liu J. Dynamic cardiac MRI reconstruction with weighted redundant Haar wavelets. Magn Reson Med. 2012;Proc. ISMRM 2012,abstract.

13 Bieri O, Markl M, Scheffler K. Analysis and compensation of eddy currents in balanced SSFP. Magn Reson Med. 2005;54:129-37.

14 Muzzarelli S, Monney P, O'Brien K, Faletra F, Moccetti T, Vogt P, Schwitter J. Quantification of aortic valve regurgitation by phase-contrast magnetic resonance in patients with bicuspid aortic valve: where to measure the flow? . Eur Heart J - CV Imaging. 2013:in press.

15 Papavassiliu T, Kühl HP, Schröder M, Süselbeck T, Bondarenko O, Böhm CK, Beek A, Hofman MMB, van Rossum AC. Effect of Endocardial Trabeculae on Left Ventricular Measurements and Measurement Reproducibility at Cardiovascular MR Imaging1. Radiology. 2005 July 1, 2005;236(1):57-64.

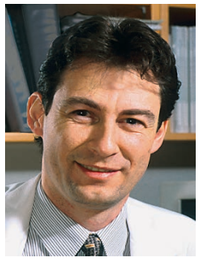

Contact

Professor Juerg Schwitter
Médecin Chef Cardiologie
Directeur du Centre de la RM
Cardiaque du CHUV
Centre Hospitalier
Universitaire Vaudois – CHUV
Rue du Bugnon 46
1011 Lausanne
Suisse
Phone: +41 21 314 0012
jurg.schwitter@chuv.ch
www.cardiologie.chuv.ch

Accelerated Segmented Cine TrueFISP of the Heart on a 1.5T MAGNETOM Aera Using *k-t*-sparse SENSE

Maria Carr[1]; Bruce Spottiswoode[2]; Bradley Allen[1]; Michaela Schmidt[2]; Mariappan Nadar[4]; Qiu Wang[4]; Jeremy Collins[1]; James Carr[1]; Michael Zenge[2]

[1]Northwestern University, Feinberg School of Medicine, Chicago, IL, USA
[2]Siemens Healthcare
[3]Siemens Corporate Technology, Princeton, United States

Introduction

Cine MRI of the heart is widely regarded as the gold standard for assessment of left ventricular volume and myocardial mass and is increasingly utilized for assessment of cardiac anatomy and pathology as part of clinical routine. Conventional cine imaging approaches typically require 1 slice per breath-hold, resulting in lengthy protocols for complete cardiac coverage. Parallel imaging allows some shortening of the acquisition time, such that 2–3 slices can be acquired in a single breath-hold. In cardiac cine imaging artifacts become more prevalent with increasing acceleration factor. This will negatively impact the diagnostic utility of the images and may reduce accuracy of quantitative measurements. However, regularized iterative reconstruction techniques can be used to considerably improve the images obtained from highly undersampled data. In this work, L1-regularized iterative SENSE as proposed in [1] was applied to reconstruct under-sampled *k*-space data. This technique* takes advantage of the de-noising characteristics of Wavelet regularization and promises to very effectively suppress subsampling artifacts. This may allow for high acceleration factors to be used, while diagnostic image quality is preserved.

The purpose of this study was to compare segmented cine TrueFISP images from a group of volunteers and patients using three acceleration and reconstruction approaches: iPAT factor 2 with conventional reconstruction; T-PAT factor 4 with conventional reconstruction; and T-PAT factor 4 with iterative *k-t*-sparse SENSE reconstruction.

Technique

Cardiac MRI seems to be particularly well suited to benefit from a group of novel image reconstruction methods known as compressed sensing [2] which promise to significantly speed up data acquisition. Compressed sensing methods were introduced to MR imaging [3, 4] just a few years ago and have since been successfully combined with parallel imaging [5, 6]. Such methods try to utilize the

*Work in progress: The product is still under development and not commercially available yet. Its future availability cannot be ensured.

Table 1: MRI conventional and iterative imaging parameters

Parameters	Conventional iPAT 2	Conventional T-PAT 4	Iterative T-PAT 4
Iterative recon	No	No	Yes
Parallel imaging	iPAT2 (GRAPPA)	TPAT4	TPAT4
TR/TE (ms)	3.2 / 1.6	3.2 / 1.6	3.2 / 1.6
Flip angle (degrees)	70	70	70
Pixel size (mm²)	1.9 × 1.9	1.9 × 1.9	1.9 × 1.9
Slice thickness (mm)	8	8	8
Temp. res. (msec)	38	38	38
Acq. time (sec)	7	3.2	3.2

1

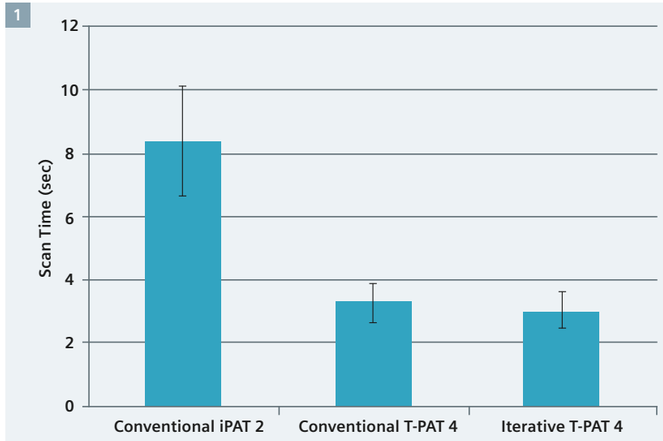

1 Single slice scan time in patients and volunteers. There was a statistically significant reduction in scan time compared to the standard iPAT2 for both TPAT4 acceleration and iterative reconstruction TPAT4 acceleration.

2

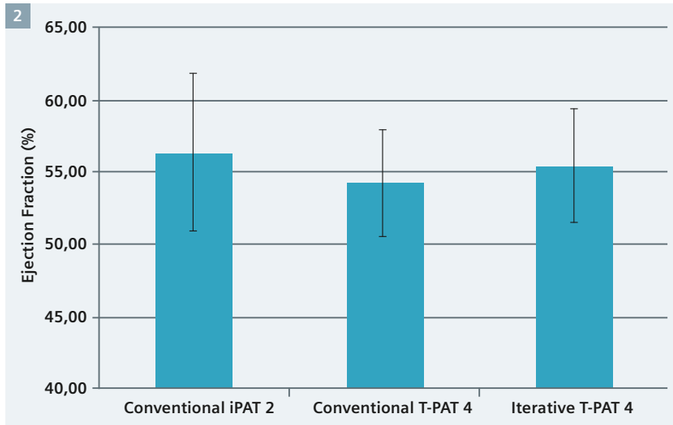

2 Ejection fraction in volunteers. Quantitatively measured ejection fractions were comparable across all three techniques.

full potential of image compression during the acquisition of raw input data. In the case of highly subsampled input data, a non-linear iterative optimization avoids sub-sampling artifacts during the process of image reconstruction. The resulting images represent the best solution consistent with the input data, which have a sparse representation in a specific transform domain. In the most favorable case, residual artifacts are not visibly perceptible or are diagnostically irrelevant.

As outlined by Liu et al. in [1], the image reconstruction can be formulated as an unconstrained optimization problem. In the current implementation, this optimization is solved using a Nesterov-type algorithm [7]. The L1-regularization with a redundant Haar transform is efficiently solved using a Dykstra-type algorithm [8]. This allowed a smooth integration into the current MAGNETOM platform and, therefore, facilitates a broad clinical evaluation.

Materials and methods

Nine healthy human volunteers (57.4 male/56.7 female) and 20 patients (54.4 male/40.0 female) with suspected cardiac disease were scanned on a 1.5T MAGNETOM Aera system under an approved institutional review board protocol. All nine volunteers and 16 patients were imaged using segmented cine TrueFISP sequences with conventional GRAPPA factor 2 acceleration (conventional iPAT 2) T-PAT factor 4 acceleration (conventional T-PAT 4), and T-PAT factor 4 acceleration with iterative *k-t*-sparse SENSE reconstruction (iterative T-PAT 4). The remaining 4 patients were scanned using only conventional iPAT 2 and iterative T-PAT 4 techniques. Note that the iterative technique is fully integrated into the standard reconstruction environment.

The imaging parameters for each imaging sequence are provided in Table 1. All three sequences were run in 3 chamber and 4 chamber views, as well as a stack of short axis slices.

Quantitative analysis was performed on all volunteer data sets at a *syngo* MultiModality Workplace (Leonardo) using Argus post-processing software (Siemens Healthcare, Erlangen, Germany) by an experienced cardiovascular MRI technician. Ejection fraction, end-diastolic volume, end-systolic volume, stroke volume, cardiac output, and myocardial mass were calculated. In all volunteers and patients,

3

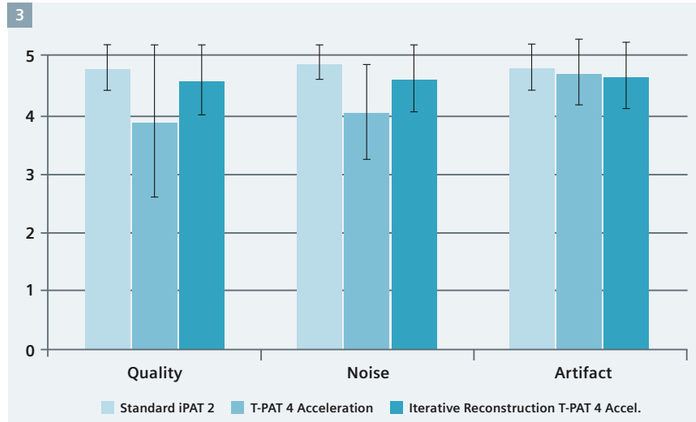

3 Qualitative scores in patients and volunteers. Image quality was highest and noise and artifact were lowest with iterative T-PAT 4 and conventional iPAT 2 compared to conventional T-PAT 4.

blinded qualitative scoring was performed by a radiologist using a 5 point Likert scale to assess overall image quality (1 – non diagnostic; 2 – poor; 3 – fair; 4 – good; 5 – excellent). Images were also scored for artifact and noise (1 – severe; 2 – moderate; 3 – mild; 4 – trace; 5 – none).

All continuous variables were compared between groups using an unpaired t-test, while ordinal qualitative variables were compared using a Wilcoxon signed-rank test.

Results

All images were acquired successfully and image quality was of diagnostic quality in all cases. The average scan time per slice for conventional iPAT 2, conventional T-PAT 4 and iterative T-PAT 4 were for patients 7.7 ± 1.5 sec, 5.6 ± 1.5 sec and 2.9 ± 1.5 sec and for the volunteers 9.8 ± 1.5 sec, 3.2 ± 1.5 sec and 3.0 ± 1.5 sec, respectively. The results in scan time are illustrated in Figure 1. In both patients and volunteers, conventional iPAT 2 were significantly longer than both conventional T-PAT 4 and iterative T-PAT 4 techniques ($p < 0.001$ for each group).

The results for ejection fraction (EF) for all three imaging techniques are provided in Figure 2. The average EF for conventional T-PAT 4 was slightly lower than that measured for conventional iPAT 2 and iterative T-PAT, but the group size is relatively small (9 subjects) and this difference was not significant ($p = 0.34$ and $p = 0.22$ respectively).There was no statistically significant difference in ejection fraction between the conventional iPAT 2 and the iterative T-PAT 4 sequences ($p = 0.48$).

The results for image quality, noise and artifact are provided in Figure 3. The iterative T-PAT 4 images had comparable image quality, noise and artifact scores compared to the conventional iPAT 2 images. The conventional T-PAT 4 images had lower image quality, more artifacts and higher noise compared to the other techniques.

Figures 4 and 5 show an example of 4-chamber and mid-short axis images from all three techniques in a patient with basal septal hypertrophy. In both series', the conventional iPAT 2 and iterative T-PAT 4 images are comparable in quality, while the conventional T-PAT 4 image is visibly noisier.

Discussion

This study compares a novel accelerated segmented cine TrueFISP technique to conventional iPAT 2 cine TrueFISP and T-PAT 4 cine TrueFISP in a cohort of normal subjects and patients. The iterative reconstruction technique provided comparable measurements of ejection fraction to the clinical gold standard (conventional iPAT 2). The accelerated segmented cine TrueFISP with T-PAT 4, which was used as comparison technique, produced slightly lower EF values compared to the other techniques, although this was not found to be statistically significant. The iterative reconstruction produced comparable image quality, noise and artifact scores to the conventional reconstruction using iPAT 2. The conventional T-PAT 4 technique had lower image quality and higher noise scores compared to the other two techniques.

The iterative T-PAT 4 segmented cine technique allows for greater than 50% reduction in acquisition time for comparable image quality and spatial resolution as the clinically used iPAT 2 cine TrueFISP technique. This iterative technique could be extended to permit complete heart coverage in a single breath-hold thus greatly simplifying and shortening routine clinical cardiac MRI protocols, which has been one of the biggest obstacles to wide acceptance of cardiac MRI. With a shorter cine acquisition, additional advanced imaging techniques, such as perfusion and flow, can be more readily added to patient scans within a reasonable protocol length.

There are currently some limitations to the technique. Firstly, the use of SENSE implies that aliasing artifacts can occur if the field-of-view is smaller than the subject, which is sometimes difficult to avoid in the short axis orientation. But a solution to this is promised to be part of a future release of the current prototype. Secondly, the image reconstruction times of the current implementation seems to be prohibitive for routine clinical use. However, we anticipate future algorithmic improvements with increased computational power to reduce the reconstruction time to clinically acceptable values.

Of course, iterative reconstruction techniques are not just limited to cine imaging of the heart. Future work may see this technique applied to time intense techniques such as 4D flow phase contrast MRI and 3D coronary MR angiography, making them more clinically applicable. Furthermore, higher acceleration rates might be achieved by using an incoherent sampling pattern [9].

With sufficiently high acceleration, the technique can also be used effectively for real time cine cardiac imaging in patients with breath-holding difficulties or arrhythmia. Figure 6 shows that real-time acquisition with T-PAT 6 and *k-t* iterative reconstruction still results in excellent image quality.

In conclusion, cine TrueFISP of the heart with inline *k-t*-sparse iterative reconstruction is a promising technique for obtaining high quality cine images at a fraction of the scan time compared to conventional techniques.

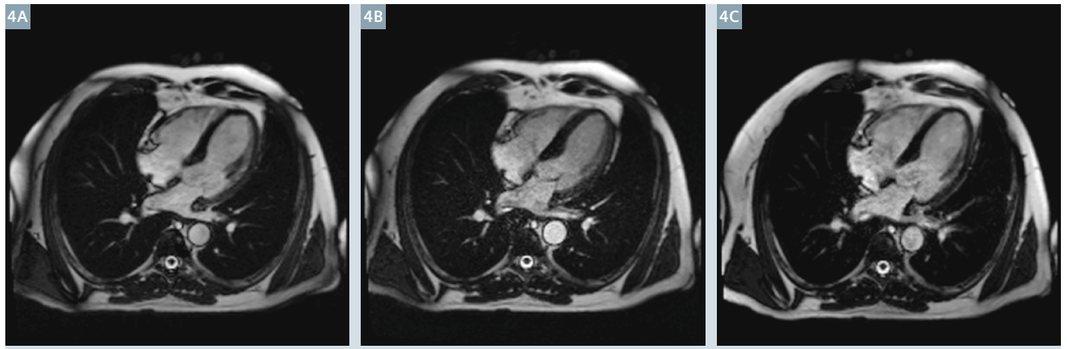

4 Four chamber cine TrueFISP from a normal volunteer. **(4A)** Conventional iPAT 2, acquisition time 8 s. **(4B)** Conventional T-PAT 4, acquisition time 3 seconds. **(4C)** Iterative T-PAT 4, acquisition time 3 seconds.

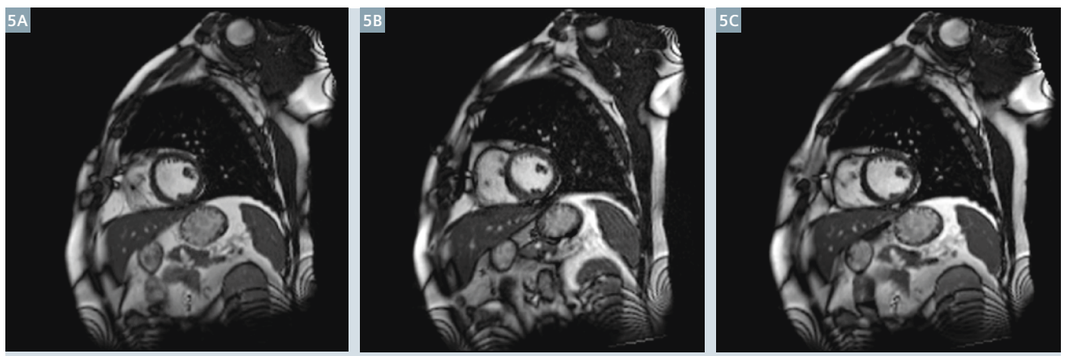

5 End-systolic short axis cine TrueFISP images from a patient with a history of myocardial infarction. A metal artifact from a previous sternotomy is noted in the sternum. There is wall thinning in the inferolateral wall with akinesia on cine views, consistent with an old infarct in the circumflex territory. **(5A)** Conventional iPAT 2, **(5B)** conventional T-PAT 4, **(5C)** iterative T-PAT 4.

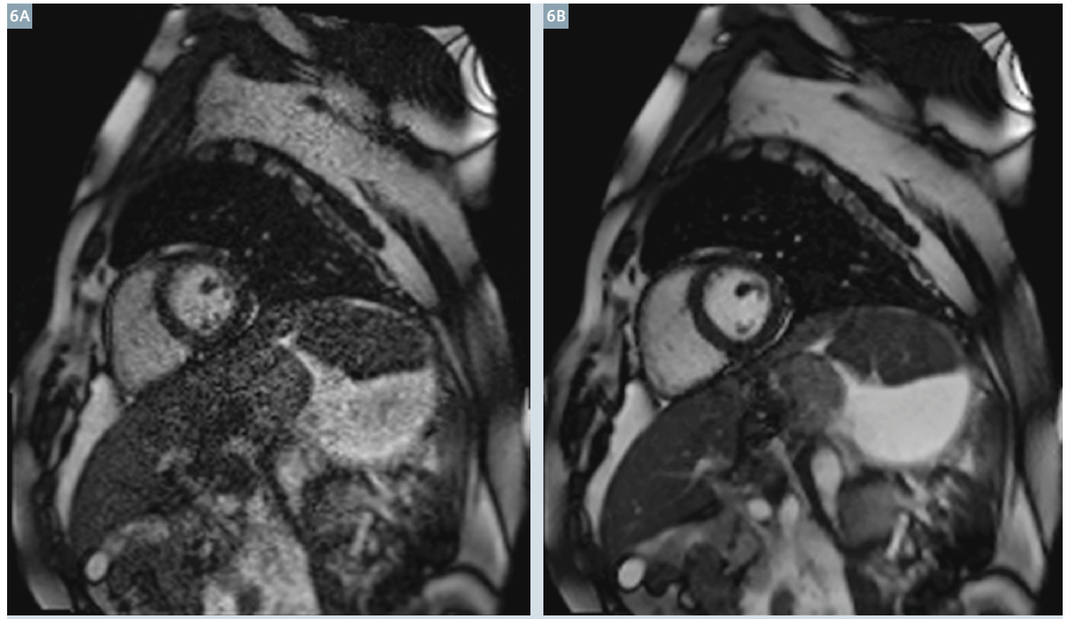

6 Real-time cine TrueFISP T-PAT 6 images reconstructed using **(6A)** conventional, and **(6B)** iterative techniques.

Acknowledgement

The authors would like to thank Judy Wood, Manger of the MRI Department at Northwestern Memorial Hospital, for her continued support and collaboration with our ongoing research through the years. Secondly, we would like to thank the magnificent Cardiovascular Technologist's Cheryl Jarvis, Tinu John, Paul Magarity, Scott Luster for their patience and dedication to research. Finally, the Resource Coordinators that help us make this possible Irene Lekkas, Melissa Niemczura and Paulino San Pedro.

References

1 Liu J, Rapin J, Chang TC, Lefebvre A, Zenge M, Mueller E, Nadar MS. Dynamic cardiac MRI reconstruction with weighted redundant Haar wavelets. In Proceedings of the 20th Annual Meeting of ISMRM, Melbourne, Australia, 2002. p 4249.

2 Candes EJ, Wakin MB. An Introduction to compressive sampling. IEEE Signal Processing Magazine 2008. 25(2):21-30. doi: 10.1109/MSP.2007.914731.

3 Block KT, Uecker M, Frahm J. Undersampled Radial MRI with Multiple Coils. Iterative Image Reconstruction Using a Total Variation Constraint. Magn Reson Med 2007. 57(6):1086-98.

4 Lustig M, Donoho D, Pauly JM. Sparse MRI: The application of compressed sensing for rapid MR imaging. Magn Reson Med 2007. 58(6):1182-95.

5 Liang D, Liu B, Wang J, Ying L. Accelerating SENSE using compressed sensing. Magn Reson Med 2009. 62(6):154-84. doi: 10.1002/mrm.22161.

6 Lustig M, Pauly, JM. SPIRiT: Iterative self-consistent parallel imaging reconstruction from arbitrary k-space. Magn Reson Med 2010. 64(2):457-71. doi: 10.1002/mrm.22428.

7 Beck A, Teboulle M. A fast iterative shrinkage-thresholding algorithm for linear inverse problems. SIAM J Imaging Sciences 2009. 2(1): 183-202.

8 Dykstra RL. An algorithm for restricted least squares regression. J Amer Stat Assoc 1983 78(384):837-842.

9 Schmidt M, Ekinci O, Liu J, Lefebvre A, Nadar MS, Mueller E, Zenge MO. Novel highly accelerated real-time CINE-MRI featuring compressed sensing with *k-t* regularization in comparison to TSENSE segmented and real-time Cine imaging. J Cardiovasc Magn Reson 2013. 15(Suppl 1):P36.

Contact

Maria Carr, RT (CT)(MR)
CV Research Technologist
Department of Radiology
Northwestern University
Feinberg School of Medicine
737 N. Michigan Ave.
Suite 1600
Chicago, IL 60611
USA
Phone: +1 312-926-5292
m-carr@northwestern.edu

Combined ^{18}F-FDG PET and MRI Evaluation of a case of Hypertrophic Cardiomyopathy Using Simultaneous MR-PET

Ihn-ho Cho, M.D.; Eun-jung Kong, M.D.

Department of Nuclear Medicine, Yeungnam University Hospital, Daegu, South Korea

Introduction

Hypertrophic cardiomyopathy (HCM) is a common condition causing left ventricular outflow obstruction, as well as cardiac arrhythmias. Cardiac MRI is a key modality for evaluation of HCM. Apart from estimating left ventricular (LV) wall thickness, LV function and aortic flow, MRI is capable of estimating the late gadolinium enhancement in affected myocardium, which has been shown to have a direct correlation with incidence and severity of arrhythmias in HCM [1]. In patients with HCM, late gadolinium enhancement (LGE) on CE-MRI is presumed to represent intramyocardial fibrosis. PET myocardial perfusion studies have shown slight impairment of myocardial blood flow with pharmacological stress in hypertrophic myocardium in HCM, presumably related to microvascular disease [2]. ^{18}F-FDG PET has been sporadically studied in HCM, mostly for evaluation of the metabolic status of the hypertrophic myocardial segment, especially after interventions such as transcoronary ablation of septal hypertrophy (TASH) [3] or to demonstrate partial myocardial fibrosis [4]. This clinical example illustrates the value of integrated simultaneous ^{18}F-FDG PET and MRI acquisition performed on the Biograph mMR system.

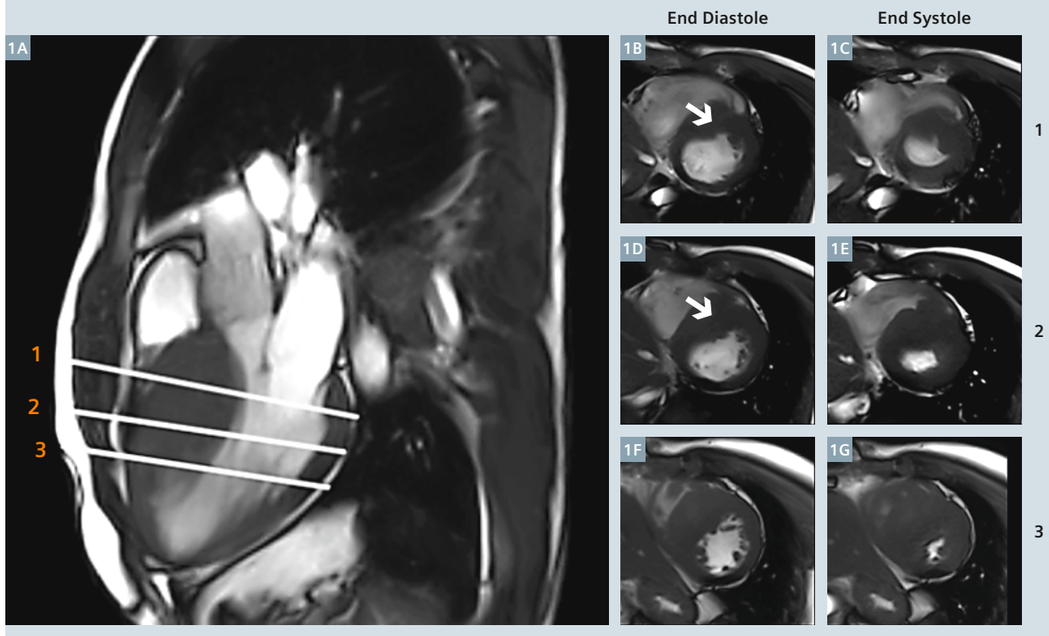

1 Short-axis views of end diastole and end systole at 3 different sections in the left ventricle obtained from gated TrueFISP cine MRI acquisitions performed on Biograph mMR. Note the thick hypertrophic septum (white arrow), which demonstrates the degree of asymmetric septal hypertrophy.

Reprinted from MAGNETOM Flash 5/2013

Patient history

A 25-year-old man presented to the cardiology department with incidental ECG abnormality after fractures to his left 2nd and 4th fingers. Although he had not consulted a doctor, he had been suffering from mild dyspnea with chest discomfort at rest and exacerbation at exercise since May 2012. Echocardiography revealed non-obstructive hypertrophic cardiomyopathy (Maron III) with trivial MR. The patient was referred for a simultaneous MR-PET study for ^{18}F-FDG PET and cardiac MRI with Gadolinium (Gd) contrast for evaluation of the morphological and metabolic status of the hypertrophic myocardium.

The patient was injected with 10 mCi ^{18}F-FDG following glucose loading. Simultaneous MR-PET study performed on a Biograph mMR was started one hour following tracer injection. Following standard Dixon sequence acquisition for attenuation correction, the comprehensive cardiac MRI sequences were acquired including MR perfusion after Gd contrast infusion, as well as post contrast late Gd enhancement studies. Static ^{18}F-FDG PET was acquired simultaneously during the MRI acquisition.

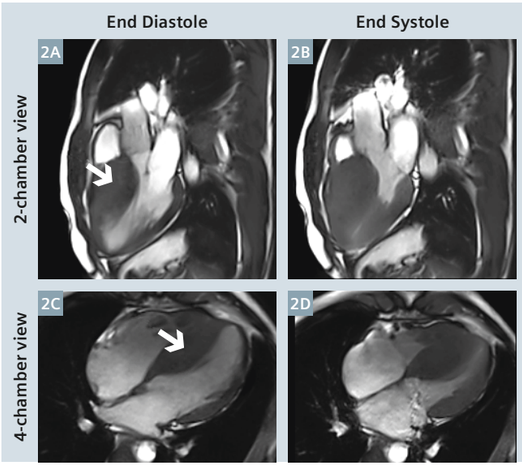

2 End diastolic and end systolic views of 2-chamber and 4-chamber views obtained from gated cine TrueFISP acquisitions showing thickness of the asymmetric septal hypertrophy (white arrow).

Discussion

The late Gd enhancement within the hypertrophic septum along with the non-uniform glucose metabolism demonstrated by the patchy ^{18}F-FDG uptake within the hypertrophic septum exactly corresponding to the area of Gd enhancement reflect myocardial fibrosis within the asymmetric septal hypertrophy. Myocardial fibrosis and the presence of late Gd enhancement on MRI has been shown to be associated with increased risk of cardiac arrhythmia [1] as evident from the symptoms of this patient.

Simultaneous MR-PET acquisition provides combined acquisition of both modalities, thereby ensuring accurate fusion between morphological and functional images due to simultaneous PET acquisition for every MR sequence. The exact coregistration of the patchy ^{18}F-FDG uptake in the area of Gd enhancement within the hypertrophic upper septum reflects the advantage of simultaneous acquisition.

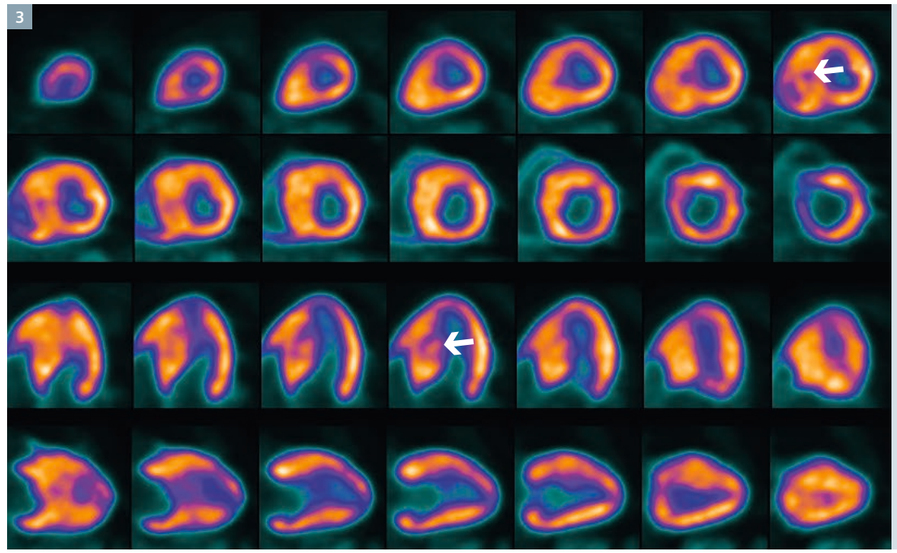

3 Static ^{18}F-FDG PET images in short-axis, horizontal long-axis and vertical long-axis views demonstrating normal uptake in the LV myocardium except the non-uniform uptake pattern in the hypertrophied septum (white arrows). LV cavity size appears normal.

Reprinted from MAGNETOM Flash 5/2013

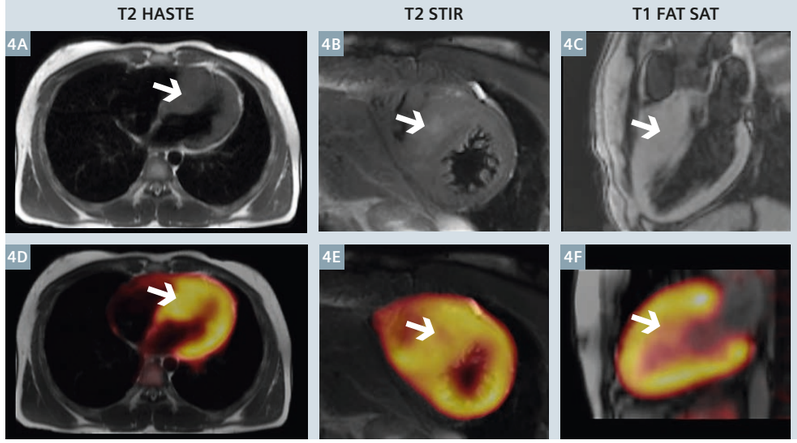

4

Transverse, short-axis and vertical long-axis MR and fused MR-PET images show hypertrophied septum (white arrows) and normal thickness of rest of left ventricular myocardium with corresponding normal ^{18}F-FDG uptake. The T2-weighted STIR (fat suppression) image shows slight hyperintensity in the middle of the hypertrophied septum which shows corresponding non-uniformity in ^{18}F-FDG uptake.

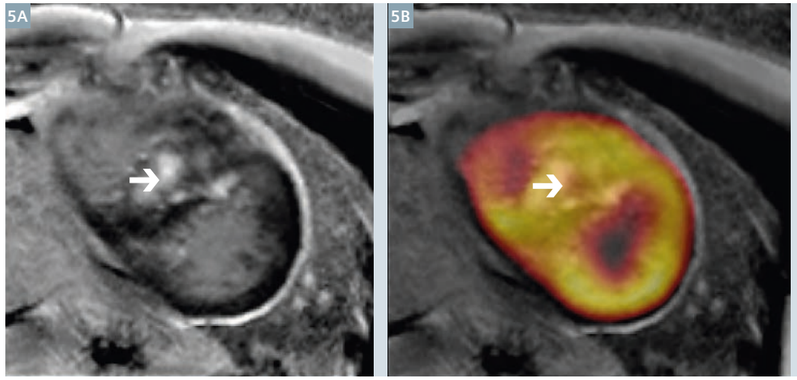

5

Post-contrast MR short-axis images demonstrate late Gd enhancement within the hypertrophied septum (white arrow), which shows corresponding non-uniform patchy uptake of ^{18}F-FDG.

References

1 Rubinstein et al. Characteristics and Clinical Significance of Late Gadolinium Enhancement by Contrast-Enhanced Magnetic Resonance Imaging in Patients With Hypertrophic Cardiomyopathy. Circ Heart Fail. 2010;3:51-58.

2 Bravo et al. PET/CT Assessment of Symptomatic Individuals with Obstructive and Nonobstructive Hypertrophic Cardiomyopathy. J Nucl Med 2012; 53:407–414.

3 Kuhn et al. Changes in the left ventricular outflow tract after transcoronary ablation of septal hypertrophy (TASH) for hypertrophic obstructive cardiomyopathy as assessed by transoesophageal echocardiography and by measuring myocardial glucose utilization and. perfusion. European Heart Journal (1999) 20, 1808–1817.

4 Funabashi N et al. Partial myocardial fibrosis in hypertrophic cardiomyopathy demonstrated by ^{18}F-fluoro-deoxy-glucose positron emission tomography and multislice computed tomography. Int J Cardiol. 2006 Feb 15;107(2):284-6.

Contact

Ihn-ho Cho, M.D.
Department of Nuclear Medicine
Yeungnam University
College of Medicine
Daegu Hyunchungro 170
South Korea
nuclear126@ynu.ac.kr

Reprinted from MAGNETOM Flash 5/2013

Cardiac MRI at 3T: An Indian Experience of 80 Cases

Cardiac MRI is the main investigation modality for a wide range of clinical applications and has emerged as a virtual 'one-stop-shop' for imaging conditions such as Cardiomyopathies.

CMR has added uniquely to the methods for non-invasive assessment of myocardial viability by a combination of cine imaging and delayed hyper-enhancement. CMR provides excellent depiction of pericardium in conditions such as pericarditis, pericardial effusions, and masses. It provides optimal assessment of the location, functional characteristics, and soft tissue features of cardiac tumors, allowing accurate differentiation of benign and malignant lesions.

MRI is ideally suited to serve as the primary imaging modality in patients with congenital heart disease due its non-invasive and biologically harmless nature, and its ability to provide accurate anatomical and functional information. Several investigators have confirmed the SNR advantages of CMR at 3T. These indicate an overall quantitative improvement in SNR and CNR, thus improving imaging capabilities.

Dr. Bidarkar and colleagues (Departments of Radiology and Cardiology, Jupiter Hospital, Thane, Maharashtra, India) illustrate 80 cases of cardiac MRI imaged between January 2012 and August 2013 on a 3T MAGNETOM Verio.

Read the comprehensive article

www.siemens.com/magnetom-world

Myocardial Tissue Imaging Using Simultaneous Cardiac Molecular MRI

James A. White, M.D., FRCPC

The Lawson Health Research Institute, London, Ontario, Canada

Molecular MRI in London Ontario

The Lawson Health Research Institute (the "Lawson") is located within St. Joseph's Healthcare in London Ontario, and is affiliated with Western University. This group received the first Biograph mMR in Canada in March 2012. With strong existing research groups in MRI and nuclear medicine this group is ideally positioned to drive research and innovation using this platform. In advance of the installation of the hybrid molecular MR, researchers at the Lawson had been developing novel MR-based attenuation correction methods, and novel tracer developments. In addition to the molecular MR this site has a PET-CT, a SPECT-CT, and an Inveon small animal PET as well as two 1.5T MAGNETOM Aera systems, a 16.5MeV medical cyclotron and radiochemistry facilities.

Myocardial tissue imaging

Hybrid imaging platforms incorporating PET have become available for cardiovascular imaging applications over the past decade. These platforms have been primarily aimed at providing superior tissue attenuation correction of the emitted photon signal and to provide spatial anatomic registration for the localization of abnormal tracer signal. While this has resulted in substantial improvements in the clinical performance of cardiac PET, the exploitation of complementary imaging data has yet to be fully realized.

The recent availability of hybrid platforms allows for an expansive range of PET applications to be explored. For example the capacity of cardiovascular MRI to provide complementary 2D and 3D morphological data with excellent soft tissue contrast and high temporal resolution is of benefit for anatomic registration and novel motion correction algorithms. However, its incremental capacity to provide exquisite tissue characterization through intrinsic tissue contrast and altered kinetics of exogenous paramagnetic contrast is of particular interest in the context of the PET imaging environment.

Clinical adoption of myocardial tissue imaging is expanding in response to mounting evidence that the 'health' of myocardium strongly modulates benefit from heart failure therapies (pharmacologic, surgical and device-based) and is predictive of future arrhythmic events among patients with ischemic and non-ischemic cardiomyopathy [1-5]. To date, this literature has focused on isolated and disparate markers of tissue health using both PET and MRI. However, within this brief report we discuss several synergies of these platforms that hold promise towards a new era of hybrid imaging for the optimal performance of myocardial tissue imaging.

1

1 The Lawson Health Research Institute.

Molecular MRI in the setting of acute ischemic injury

Among those surviving acute myocardial infarction (AMI), appropriate myocardial healing is believed to be reliant upon a highly choreographed process of early inflammatory cell invasion, collagen degredation, debris removal by activated macrophages, and myofibroblast proliferation with reconstitution of a new collagen matrix. While

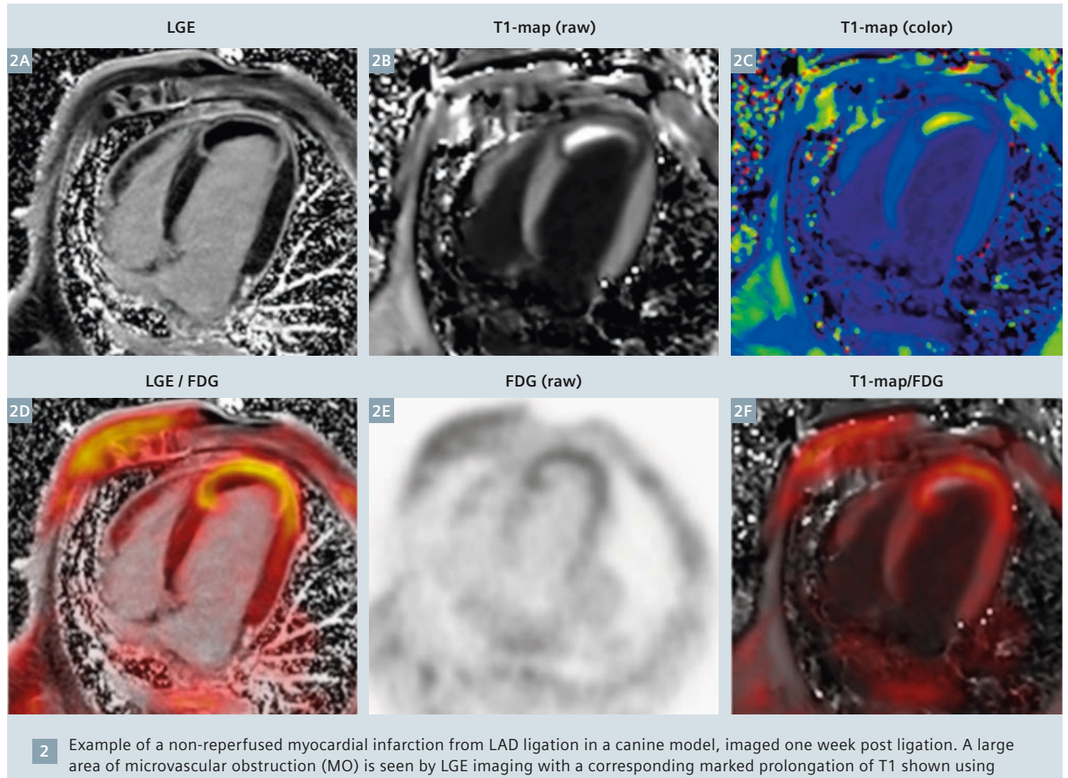

2 Example of a non-reperfused myocardial infarction from LAD ligation in a canine model, imaged one week post ligation. A large area of microvascular obstruction (MO) is seen by LGE imaging with a corresponding marked prolongation of T1 shown using MOLLI-based T1 mapping. Simultaneously acquired FDG imaging (binned to cardiac phase) has been fused to both LGE imaging and raw T1 map and illustrates a marked reduction in inflammation within the region of MO. There is intense inflammatory activity evident within the perfused infarct rim.

such findings can be characterized histologically, our capacity to quantify markers of the inflammatory process *in vivo*, and evaluate influences of its modulation on the remodeling process has been limited.

We have started examining this process in a canine infarct model using the Biograph mMR 3T-PET platform using simultaneous 3D LGE / ^{18}F-FDG imaging, the latter imaged following normal myocardial glucose metabolism using intravenous heparin and lipid infusion. In these experiments we have focused on evaluating the influence of microvascular obstruction (MO) on mitigating appropriate inflammatory cell recruitment to the infarct core – a postulated mechanism of how MO may adversely impact on left ventricular remodeling post infarct. Figure 2 illustrates how the region of MO can be elegantly visualized using both LGE imaging and T1 mapping CMR techniques. ^{18}F-FDG imaging shows intense inflammatory activity within the perfused infarct rim, however a marked reduction in activity is seen in regions of MO. This imaging may therefore provide novel insights towards mechanisms by which MO contributes to adverse outcomes following AMI, and offers a new tool to evaluate therapies aimed at modulation of this pathway.

Molecular MRI in the setting of acute non-ischemic (inflammatory) injury

Both PET and CMR have been investigated for their diagnostic accuracy in the setting of suspected inflammatory cardiomyopathy – particularly among patients with known pulmonary Sarcoid. While their respective diagnostic performance has been compared in the past, this remains inappropriate, as the information gathered and interpreted from each technique could not be more unique. PET imaging (typically performed using ^{18}F-FDG following prolonged fasting, fatty meal consumption and intravenous heparin to suppress normal myocardial glucose utilization) exploits the hypermetabolic signal of activated inflammatory cells (i.e. macrophages) and therefore indicates disease 'activity' among patients with active cardiac Sarcoid. In contrast, LGE imaging indicates regions of mature granulomatous fibrosis among patients with prior or current cardiac Sarcoid. Therefore, these two commonly employed diagnostic techniques provide complementary but unique information.

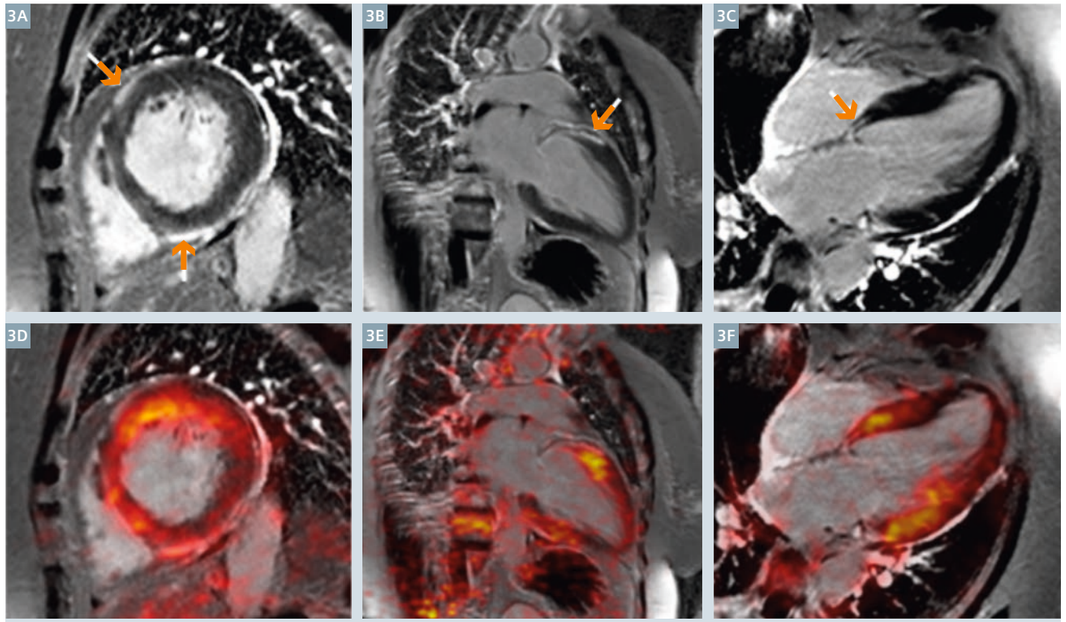

3 72-year-old female with suspected new-onset heart failure and non-sustained ventricular tachycardia and prior history of biopsy-proven systemic Sarcoid. Top rows show late gadolinium enhancement (LGE) imaging with characteristic sub-epicaridal based scar (arrows), consistent with prior inflammatory injury. Lower row shows fused FDG-PET images with evidence of focal signal enhancement, consistent with active inflammation surrounding regions of established scar.

Figure 3 illustrates the capacity of hybrid MR and PET to spatially register these techniques using simultaneously acquired data, and potentially improve diagnostic accuracy while expanding our understanding of disease pathophysiology. In this case of a 72-year-old female presenting with heart failure and non-sustained ventricular tachycardia we can identify a leading edge of inflammation (intense FDG uptake) with a trailing edge of irreversible injury or 'scar' (indicated by hyperenhancement on LGE imaging) at the sub-epicardial zone. This approach ushers in a new era of imaging for inflammatory-mediated disease where a more complete spectrum of disease activity can be visualized in a single, spatially registered examination.

Molecular MRI in the setting of non-acute myocardial disease

Another clinical setting where MR and PET have established their respective roles for therapeutic decision-making is for the assessment of tissue viability in chronic ischemic cardiomyopathy. Evidence supports that both the regional reduction of FDG signal [6, 7] and regional scar transmurality by LGE are strongly predictive of absence of functional recovery following coronary revascularization. The performance of these studies are therefore commonly considered to be mutually exclusive, with absence of FDG signal being the *sine qua non* of myocardial scar, and the lack of scar by LGE imaging being equivalent to tissue health. However, it is recognized that the spatial resolution and signal-to-noise of LGE imaging is superior to FDG for the detection of subendocardial scar, and also for the characterization of tissue viability among those with marked thinning of the ventricular wall [8]. Conversely, FDG-PET based metabolic abnormalities can be documented within tissue that fails to demonstrate myocardial scar on LGE MRI, lack of FDG uptake being predictive of absence of functional recovery. Accordingly, the marriage of PET-based metabolic imaging and LGE-based scar imaging may provide a more robust platform for the prediction of improved outcomes following coronary revascularization.

In figure 4 we see a 42-year-old male referred for viability imaging prior to coronary artery bypass surgery late following myocardial infarction. Cine imaging shows a large region of thinned and akinetic myocardium in the distribution of the left anterior descending artery, this territory demonstrating varying degrees of transmural scar following gadolinium administration. Simultaneous MR and PET with ^{18}F FDG imaging shows metabolic activity within non-scarred regions surrounding the infarct zone and normal metabolic tracer activity within remote myocardium.

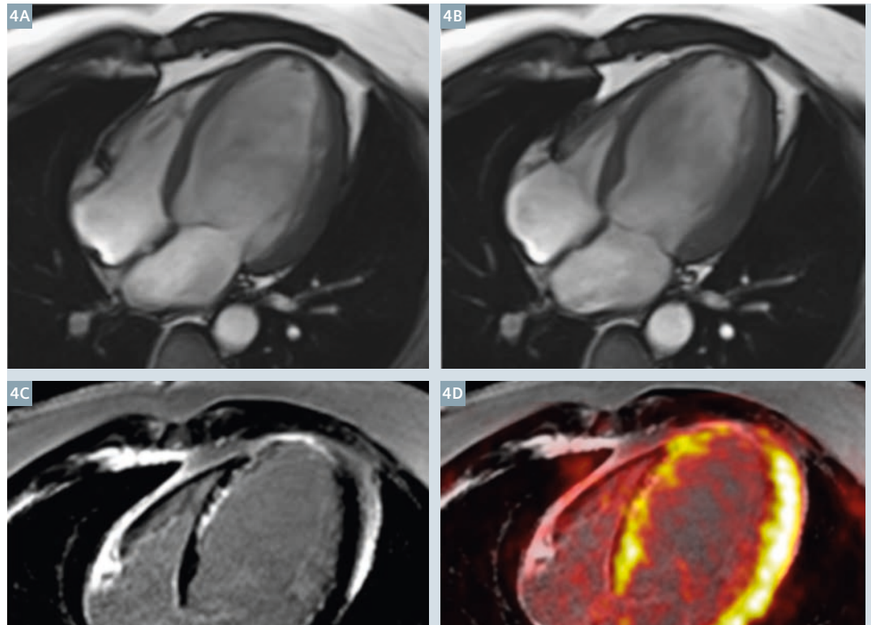

4 42-year-old male with large anterior wall myocardial infarction being considered for surgical revascularization in the setting of triple vessel disease. Cine MRI shows akinesia of the septum and apex with a reduced ejection fraction of 32%. Late gadolinium enhancement (LGE) imaging shows a large infarct of the LAD territory with variable scar transmurality ranging from 25% to 100% throughout the infarct region. FDG-PET imaging, shown fused with LGE imaging, shows matched reductions in metabolic tracer uptake.

References

1 Gulati A, Jabbour A, Ismail TF, Guha K, Khwaja J, Raza S, Morarji K, Brown TD, Ismail NA, Dweck MR, Di Pietro E, Roughton M, Wage R, Daryani Y, O'Hanlon R, Sheppard MN, Alpendurada F, Lyon AR, Cook SA, Cowie MR, Assomull RG, Pennell DJ, Prasad SK. Association of fibrosis with mortality and sudden cardiac death in patients with nonischemic dilated cardiomyopathy. JAMA. 2013;309:896-908.

2 Gao P, Yee R, Gula L, Krahn AD, Skanes A, Leong-Sit P, Klein GJ, Stirrat J, Fine N, Pallaveshi L, Wisenberg G, Thompson TR, Prato F, Drangova M, White JA. Prediction of arrhythmic events in ischemic and dilated cardiomyopathy patients referred for implantable cardiac defibrillator: Evaluation of multiple scar quantification measures for late gadolinium enhancement magnetic resonance imaging. Circ Cardiovasc Imaging. 2012;5:448-456.

3 Kwon DH, Halley CM, Carrigan TP, Zysek V, Popovic ZB, Setser R, Schoenhagen P, Starling RC, Flamm SD, Desai MY. Extent of left ventricular scar predicts outcomes in ischemic cardiomyopathy patients with significantly reduced systolic function: A delayed hyperenhancement cardiac magnetic resonance study. JACC Cardiovasc Imaging. 2009;2:34-44.

4 Klem I, Shah DJ, White RD, Pennell DJ, van Rossum AC, Regenfus M, Sechtem U, Schvartzman PR, Hunold P, Croisille P, Parker M, Judd RM, Kim RJ. Prognostic value of routine cardiac magnetic resonance assessment of left ventricular ejection fraction and myocardial damage: An international, multicenter study. Circ Cardiovasc Imaging. 2011;4:610-619.

5 Neilan TG, Coelho-Filho OR, Danik SB, Shah RV, Dodson JA, Verdini DJ, Tokuda M, Daly CA, Tedrow UB, Stevenson WG, Jerosch-Herold M, Ghoshhajra BB, Kwong RY. CMR quantification of myocardial scar provides additive prognostic information in nonischemic cardiomyopathy. JACC Cardiovasc Imaging. 2013;6:944-954.

6 Romero, J, Xue X, Gonzalez W, Garcia MJ. CMR Imaging Assessing Viability in Patients With Chronic Ventricular Dysfunction Due to Coronary Artery Disease: A Meta-Analysis of Prospective Trials. J. Amer. Coll Cardiol Img 2012;5:494 -508.

7 Lee Fong Ling, Thomas H. Marwick, Demetrio Roland Flores, Wael A. Jaber, Richard C. Brunken, Manuel D. Cerqueira and Rory Hachamovitch. Identification of Therapeutic Benefit from Revascularization in Patients With Left Ventricular Systolic Dysfunction : Inducible Ischemia Versus Hibernating Myocardium. Circ Cardiovasc Imaging 2013;6;363-372.

8 Klein C, Nekolla SG, Bengel FM, Momose M, Sammer A, Haas F, et al. Assessment of myocardial viability with contrast-enhanced magnetic resonance imaging: Comparison with positron emission tomography. Circulation 2002;105:162-7.

Contact

James A. White, M.D., FRCPC
Robarts Research Institute
P.O. Box 5015, 100 Perth Drive
London ON, Canada
N5K 5K8
Phone: +1 519-663-5777
jawhit@ucalgary.ca

Global Business Unit

Siemens AG
Medical Solutions
Magnetic Resonance
Henkestrasse 127
DE-91052 Erlangen
Germany
Phone: +49 9131 84-0
www.siemens.com/healthcare

Local Contact Information

Asia/Pacific:
Siemens Medical Solutions
Asia Pacific Headquarters
The Siemens Center
60 MacPherson Road
Singapore 348615
Phone: +65 6490 6000

Canada:
Siemens Canada Limited
Healthcare Sector
1550 Appleby Lane
Burlington, ON L7L 6X7, Canada
Phone +1 905 315-6868

Europe/Africa/Middle East:
Siemens AG, Healthcare Sector
Henkestr. 127
91052 Erlangen, Germany
Phone: +49 9131 84-0

Latin America:
Siemens S.A., Medical Solutions
Avenida de Pte. Julio A. Roca No 516, Piso
C1067 ABN Buenos Aires, Argentina
Phone: +54 11 4340-8400

USA:
Siemens Medical Solutions USA, Inc.
51 Valley Stream Parkway
Malvern, PA 19355-1406, USA
Phone: +1 888 826-9702

Global Siemens Headquarters

Siemens AG
Wittelsbacherplatz 2
80333 Munich
Germany

Global Siemens Healthcare Headquarters

Siemens AG
Healthcare Sector
Henkestrasse 127
91052 Erlangen
Germany
Phone: +49 9131 84-0
www.siemens.com/healthcare

Order No. A91MR-1000-106C-7600 | Printed in Germany | CC MR 1839 01140.3 | © 01.14, Siemens AG

www.siemens.com/magnetom-world